

AD-A240 285



2

Final report: "Mixing and finestructure processes in the Coastal Transition Zone"

Principal Investigator: Libe Washburn
Dept. of Geography
University of California
Santa Barbara, CA 93106-4060

ONR contract number: N00014-90-J-1096

1990

DTIC
SELECTE
SEP 05 1991
S B D

DISTRIBUTION STATEMENT A
Approved for public release
Distribution Unlimited

91-09628



"Water mass subduction and the transport of phytoplankton in a coastal upwelling system"

Libe Washburn^{1,5}, David C. Kadko^{2,6},
Burton H. Jones¹, Thomas Hayward³,
P. Michael Kosro², Timothy P. Stanton⁴,
Steve Ramp⁴, and Timothy Cowles²

¹University of Southern California, Los Angeles, CA

²College of Oceanography, Oregon State University, Corvallis, OR

³Scripps Institution of Oceanography, La Jolla, CA

⁴Naval Postgraduate School, Monterey, CA

⁵now at: Dept. of Geography, University of California,
Santa Barbara, CA

⁶now at: Rosentiel School for Marine and Atmospheric Science
University of Miami, Miami, FL



Accession For	
NTIS GRA&I	<input checked="" type="checkbox"/>
DTIC TAB	<input type="checkbox"/>
Unannounced	<input type="checkbox"/>
Justification	
By <i>per letter</i>	
Distribution/	
Availability Codes	
Dist	Avail and/or Special
<i>A-1</i>	

ABSTRACT

Observations during the Coastal Transition Zone (CTZ) experiment in summer, 1988 reveal the presence of deep phytoplankton layers in a coastal upwelling system. The layers occur throughout the CTZ study area, including a strong baroclinic jet which was present over the period of the experiment. Based on a variety of bio-optical, hydrographic, and geochemical indicators, it is concluded that the water masses associated with the layers result from subduction processes. Criteria are developed to identify subducted water masses based on the beam attenuation coefficient, chlorophyll fluorescence, and distribution of light in the water column. Temperature-salinity characteristics are consistent with two source regions for the subducted layers, one near shore and a second farther offshore. Most of the layers correspond to the inshore source which is apparently distributed alongshore. Subducted water masses are found in all 6 grid surveys of the CTZ experiment and probably result from a variety of physical processes. One of these is flow along sloping isopycnal surfaces due to advection and mixing processes. Advection timescales for flow out the axis of the jet range from a few days to a few weeks, depending on the depth of a particular surface, and the bio-optical indicators for subduction processes persist over these time scales.

1. INTRODUCTION

An unanticipated observation during the Coastal Transition Zone (CTZ) experiment is the occurrence of layers of high concentrations of phytoplankton at depths often greatly exceeding the euphotic zone. These layers are found both near shore and offshore within a productive coastal upwelling system off northern California and are often observed in a strong offshore jet that was present in the CTZ study area in 1988. We explore the hypothesis that the water masses associated with these layers originate near the surface in the euphotic zone and are subsequently transported downward by vertical circulation processes or subduction (other terms such as subsidence or downwelling are equally descriptive). The subduction hypothesis is supported by a variety of physical, biological, and geochemical indicators including ^{222}Rn , dissolved O_2 , and chlorophyll (Kadko et al. 1990).

This movement of large volumes of water out of the surface layer (euphotic zone) is potentially important to the vertical transport of heat, mass, salt, and other scalars. Furthermore, geochemical data indicate that this transport can be rapid with vertical velocities of order 20 - 30 m/day (Kadko et al. 1990). It also may result in a high vertical flux of organic carbon and represents a mechanism which could quickly remove large concentrations of phytoplankton from the euphotic zone in a productive coastal environment.

At this point, the characteristics of subducted water masses and the mechanisms leading to their subduction in a coastal region are not well understood. Some basic questions include: What are the thicknesses, horizontal extents, and volumes of subducted water masses? Are subducted water masses only associated with offshore jets or are they more widely distributed in the CTZ? Where are the source regions for the subducted water masses? Are the source regions local in the sense that subduction results from vertical sinking with little horizontal advection? Or, is horizontal advection strong enough to move subducted water masses away from the region where sinking occurs? Are subducted waters transported offshore and, if so, at what rates? What physical processes lead to subduction?

Experimentally, it is necessary to determine quantities and criteria that can be used to establish that an observed water mass has been subducted. It is also important to determine the effective decay times for various subduction indicators.

2. EXPERIMENTAL PROCEDURE

A more complete description of the shipboard observations from the CTZ experiment during the summer, 1988 is presented by

Huyer et al. (1991). Basically, the overall strategy was to sample a region of the CTZ between Pt. Reyes and Pt. Arena, California over a period of several weeks in order to observe the evolution of strong coastal jets which have been observed previously in the area (cf. Flament et al., 1985 and Davis, 1985). To do this, six hydrographic grid surveys of more or less uniform spatial coverage were made sequentially from three ships: R/V's Wecoma, Pt. Sur, and Thomas Washington (leg 1). (The sampling grids for 5 of these surveys are indicated in Fig. 4.) Due to adverse weather conditions, the entire leg 1 grid survey from the Thomas Washington could not be completed (This incomplete grid is shown in Fig 12). However, the inshore part was completed and is used here to examine near shore water properties. In addition, during leg 2 of the Thomas Washington survey, sampling was specifically directed at observing physical, biological and chemical distributions in the offshore jet with some limited sampling outside the jet (station locations are indicated by triangles in Fig. 5). The period of this "process sampling" was 18 days (4 July to 21 July) and coincided with the first two hydrographic grid surveys of the Pt. Sur which were conducted from 6 to 18 July.

Measured variables from all vessels include conductivity, temperature, depth (CTD), chlorophyll fluorescence, beam transmission and meteorological observations. Fluorometers and transmissometers were manufactured by Sea-tech, Inc. of Corvallis, Oregon and each transmissometer has a 0.25 m path length with a 660 nm wavelength light source. Rosettes with Niskin bottles were used in conjunction with the CTD instrumentation to provide bottle sampling for salinity calibration, dissolved O₂, nutrients, chlorophyll, and pigments. Continuous profiles of photosynthetically available radiation (PAR) were made from the Thomas Washington using a sensor manufactured by Bio-spherical Instruments, Inc. of San Diego, California.

3. EVIDENCE FOR SUBDUCTION

The primary evidence for subduction processes discussed here is layers of phytoplankton which are observed at depths below the euphotic zone. Because phytoplankton are green plants, they require light for photosynthesis and grow in the illuminated layers of the upper ocean. The presence of phytoplankton in the water column is detected by a combination of chlorophyll fluorescence and beam attenuation coefficient (beam c) profiles. Beam c is a quantitative measure of water column turbidity which depends upon various aspects of the particle field such as particle concentrations, size distribution, and index of refraction (cf. Jerlov, 1976; Baker and Lavelle, 1984). Vertical profiles of beam c and chlorophyll fluorescence at stations containing phytoplankton layers are highly correlated and the presence of phytoplankton in these layers is verified by bottle

samples. Such a station located 50 km west of Pt. Arena and in a region of strong southward flow is shown in Fig. 1.

Beam c values exceed 0.4 m^{-1} and the chlorophyll fluorescence signal is above the noise level almost everywhere above 190 db (Fig. 1B). The measured 1% light level here is 31 db and three distinct layers are found: 1) a near surface layer above the 1% light level where chlorophyll concentrations are as high as $8.6 \mu\text{g/l}$, 2) a deeper layer which extends from the 1% light level to about 110 db, and 3) a very deep layer with low beam c and fluorescence levels which extends from 125 to 190 db. No surface mixed layer is observed and gradients in all measured quantities extend to the surface. A weak temperature inversion is present on the upper boundary of layer 2 (Fig. 1C) and suggests that this layer is intrusive, a conclusion also supported by the T-S diagram for this station. Examples of several T-S diagrams showing an association between deep fluorescence layers and relatively warm, salty anomalies are given by Kadko et al. (1991).

A very different type of profile is typically found in offshore waters away from the jet, such as at station E-4 (Fig. 1A). A deep fluorescence layer is centered at about 93 db, well below the 60 db deep surface mixed layer, and lies just below the 1% light level at 85 db (Fig. 2A and 2B). Chlorophyll concentrations from bottle samples are about $0.5 \mu\text{g/l}$ just above and below the fluorescence peak; apparently the peak itself was missed in sampling. However, chlorophyll and fluorescence are highly correlated and nearby stations show peak concentrations of about $1 \mu\text{g/l}$. Chlorophyll layers of this type, which occur in association with the base of the euphotic zone, are common features of the California Current system (cf. Anderson, 1969 and Cullen, 1982). They may result from a number of processes such as an increase in phytoplankton biomass due to growth at the intersection of the euphotic zone and nutricline (Herbland and Voituriez, 1979). Two other possibilities are photoadaptation, where the chlorophyll per cell increases in response to low light conditions (Prezelin, 1981 and Beers et al. 1975), or variability in fluorescence yield of the phytoplankton (Kiefer, 1982). At station E-4 and nearby stations the increase in beam c indicates increased biomass while the fluorescence per unit chlorophyll, or fluorescence yield, is relatively constant throughout the water column. However, the chlorophyll per unit beam c increases with depth at E-4 and suggests that the chlorophyll content per cell or per unit biomass also increases with depth.

To objectively examine CTZ data sets for the occurrence of phytoplankton layers which may have been moved out of the euphotic zone by subduction processes, it is necessary to differentiate the deep layers like those of Fig. 1 from those which probably result from in situ photosynthesis as in Fig. 2. Furthermore, it is necessary to rule out other processes which might also result in the presence of layers of fluorescent

particles below the euphotic zone. A step in this process is to establish the relationship between the light field in the water column throughout the region and the vertical positions of layers of phytoplankton.

The penetration of light into the water column is examined by comparing vertical profiles of PAR throughout the CTZ. A total of 17 stations from legs 1 and 2 of the Thomas Washington survey, all recorded within one hour of local noon, is used to examine the variability of the light field (Fig. 3A). Stations close to local noon were chosen in order to observe the maximum penetration of light into the water column. Following Huyer et al. (1991), three regions are identified based on dynamic height (5/500 db): the jet corresponds to the range 0.82 to 0.96 m, inshore and southern waters below 0.82 m, and offshore and northern waters greater than 0.96 m. These ranges are somewhat different from those used by Huyer et al. (1991), but are more appropriate to the Thomas Washington data. Considerable variation in the depth of light penetration is found within the jet waters: typical values of the 1% light level in the most turbid waters are in the range of 20 to 30 db and are almost 80 db in the more clear waters (Fig. 3B). This depth range also spans that observed for the inshore and southern waters. Offshore waters are generally more clear with a typical 1% light level of about 85 db; much of the phytoplankton in the water column lies below this level.

Observations obtained during leg 2 of the Thomas Washington survey show that almost one fourth of the water column with high chlorophyll fluorescence levels (>1.0 volts) is found at depths below the 1% light level of the clearest offshore waters (Fig. 3C). About 6.4% occur below the 0.1% light level which ranges from about 115 to 125 db based on the three offshore profiles of Fig. 3B. The threshold fluorescence value of 1.0 v is chosen because it represents a high signal level; the noise level of the fluorometer and CTD acquisition system used on the Thomas Washington is about a factor of 4 smaller. The tail of the distribution of Fig. 3C extends down to 200 db, although layers exhibiting high fluorescence are found at depths exceeding 200 db in some of the other surveys. For stations within the jet, the fluorescence threshold used in producing the histogram of Fig. 3C corresponds to a chlorophyll concentration of about 1 $\mu\text{g}/\text{l}$ and in the offshore waters to a level of about 0.3 $\mu\text{g}/\text{l}$. The points sorted into the histogram also have beam c values exceeding 0.4 m^{-1} . Thus much of the phytoplankton lies below the euphotic zone.

4. SUBDUCTION CRITERIA

Because phytoplankton require light for growth and reproduction, it is unlikely that local production of particles by photosynthesis can account for particle layers below the euphotic zone. These correspond to the hatched regions of Fig.

3B, particularly those below the 0.1% light level. This suggests that other processes are responsible for these deep layers such as vertical circulation out of the euphotic zone, particle sinking, resuspension of bottom sediments containing chlorophyll, or diapycnal mixing. We have no microstructure measurements to assess diapycnal mixing rates and assume that this is not an important mechanism for vertical particle transport here.

The hypothesis that vertical circulation, or subduction, accounts for these layers has been investigated by Kadko et al. (1991) and is supported by a variety of indicators. In addition to high levels of chlorophyll, these layers often contain deficiencies of ^{222}Rn ($\lambda_{1/2} = 3.85$ days) with respect to ^{226}Ra activity, which indicates recent gas exchange with the atmosphere. The radon observations are perhaps the most unambiguous of all subduction indicators, since no other process can produce the deficiencies. The layers are often associated with local maxima in dissolved oxygen and often appear in water masses which are warmer and saltier than waters above and below in θ -S diagrams. All of these observations are consistent with vertical movement of water masses away from the surface. However, a limitation of these indicators is that they are based on bottle sampling and therefore have very limited vertical resolution. Furthermore, the indicator ^{222}Rn is available for a relatively small number of stations and only as part of the Thomas Washington survey. In this analysis, we focus on the distributions of chlorophyll fluorescence and beam c as subduction indicators because they can be measured to about the same vertical resolution as CTD variables and because they are available from all surveys.

The possible role of particle sinking in forming the deep fluorescent layers is difficult to assess, although a number of factors suggest that it is not the dominant process. First, oceanic phytoplankton generally tend to sink slowly at vertical velocities of less than 1 m/day (Bienfang, 1981; Bienfang and Szyper, 1982; Bienfang et al. 1982; Smayda, 1970). Observations from the Pt. Conception area of California indicate that phytoplankton sinking rates within 50 km of the upwelling center are less than 2 m/day (Bienfang, 1984). These estimates are much smaller than a vertical subduction velocity of 27 m/day obtained by Kadko et al. (1991) based on Rn^{222} samples.

Second, θ -S relationships observed in these deep layers found in offshore regions of the jet appear related to those found near shore in the euphotic zone, as is shown later. If particle sinking were dominant, then the θ -S relationship of a layer would have no correspondence to properties in the euphotic zone from which the particles were derived. The θ -S of the layer would simply be the local relationship at the time and depth at which the particle layer is observed as it sinks downward. As an additional check on the possible role of particle sinking in

forming the deep layers, the densities corresponding to layers near shore in the jet were compared with those found offshore. No consistent increase in density is observed offshore as might be expected as a result of particle sinking over the time required to advect out the jet (a few days to a few weeks, depending on the position of a layer in the water column).

Third, many of the deep regions of phytoplankton are in thin, well defined layers which are more or less Gaussian in shape (eg. Fig. 6F). A distribution of descending particles all falling at different rates (but strongly weighted toward large numbers of small particles; cf. Spinrad, 1986), for many days would tend to be spread vertically throughout the water column and would not concentrate in layers. Finally, in cross axis sections of the jet, where the station spacing is about 10 km, distributions of fluorescence and beam c approximately parallel σ_θ surfaces. This would not be expected if particle sinking across density surfaces were dominant.

It is possible that particle sinking may work in combination with subduction processes in layer formation. In near shore areas where chlorophyll concentrations are large, particle coagulation effects may be important (Jackson, 1991) and could result in much higher sinking rates, greater than 100 m/day (Smetacek, 1985). However, the coagulated particles would have to have combined effective densities equal to the seawater density at some point in the water column to remain suspended. Otherwise they would sink to the bottom.

Another possible mechanism which might result in fluorescent particles appearing below the euphotic zone is resuspension of bottom sediments containing phytoplankton. Deep nepheloid layers due to resuspension processes have been observed over the continental shelf off Oregon by Pak and Zaneveld (1977). Turbidity layers with high values of beam c are commonly observed below 100 m in all of the CTZ hydrographic data sets, particularly near shore. Typically these layers occur near the sea floor and exhibit no measurable fluorescence. However, deep turbidity layers from a few profiles exhibit very low, but measurable fluorescence signals. Comparison of signal levels indicates that the ratio of fluorescence to beam c is much lower in these bottom resuspended layers than in the phytoplankton layers higher in the water column. These layers are easily differentiated because their θ - S relationships are very different from those found anywhere in the euphotic zone and the corresponding seawater densities are much greater. Another difference between the subducted layers and these deep turbidity layers is the ratio of phaeopigment to total pigment present. In the deep turbidity layers the ratio is often larger than 0.8 while in the subducted layers it is typically less than 0.4 (separate analysis by one of the authors, BHJ)

Based on the preceding analysis, we conclude that the

phytoplankton layers observed well below the euphotic zone, which exhibit high values and correlated distributions of fluorescence and beam c , result primarily from subduction processes. However, some clarification about "well below the euphotic zone" is required. The presence of phytoplankton below the 1% light level at a specific station does not necessarily mean that the phytoplankton were not produced in situ, because the depth of light penetration can change. For example, a layer of phytoplankton might initially grow near the deepest observed 1% light level of 80 to 90 db in clear water. After this growth, energetic near-surface advection could transport a second, more shallow layer of particles, over the deeper layer and produce a much shallower 1% light level. The result would be a deep layer of phytoplankton produced in situ which is observed below the euphotic zone. Other scenarios might also produce a similar situation. For this reason we generally limit our analysis to those layers found below the deepest 0.1% light levels which are found in clear, offshore waters. We have used a pressure of 120 db, about the midpoint of the range in 0.1% light levels in offshore waters (Fig. 3C), to represent this point in the water column. While this is a very restrictive criteria it does reduce the possibility that the observed particles result from in situ photosynthesis.

To objectively search each of the CTZ data sets for subducted water masses we applied three criteria based on the preceding analysis. If all three of the following criteria are satisfied, we consider the water mass to have been subducted. The criteria are: 1) pressure > 120 db, 2) beam $c > 0.4 \text{ m}^{-1}$, and 3) fluorescence signal exceeds the instrumental noise level. For these data, a beam c threshold of 0.4 m^{-1} or larger is found to differentiate turbid layers from more clear ambient waters. Minimum observed levels of beam c in individual profiles from all of the data sets fall in the range $0.35 - 0.40 \text{ m}^{-1}$ and are taken to be representative of the effective clear water values of beam c (c_w). This range of c_w falls within that given by Lavelle and Baker (1987) of $0.31 - 0.42 \text{ m}^{-1}$. The range is also comparable to two experimental results for c_w presented by Jerlov (1976, Table XIII): 0.319 m^{-1} and 0.385 m^{-1} (interpolated to 660nm).

The threshold fluorescence signal level had to be determined individually for each of the surveys because the effective noise level for each fluorometer and CTD data acquisition system was different. The procedure for determining this threshold is basically subjective and is based on comparing signal levels in fluorescent layers with minimum observed levels which are taken to be the instrumental noise level. Minimum signal thresholds are derived from all of the survey data and are used in identifying subducted water masses. It proved impractical to use a uniform chlorophyll or total pigment concentration as a criteria for these data because of high scatter in the observed relationship between fluorescence voltage and pigment

concentrations derived from bottle samples. Much of this scatter is apparently due to regional differences in the regression coefficients and may result from differences in phytoplankton species composition (Hood, 1990).

To search for subducted water masses, all of the CTZ data sets were sorted based on the criteria developed above. Profiles from all surveys identified as containing subducted layers were individually examined to verify that noise spikes or other data problems were not present. This sorting procedure also identified a few layers near the sea floor with relatively high beam c, but very weak fluorescence levels that barely exceeded the threshold. Water properties of these points are typical of the ambient deep water and they are usually found at depths exceeding 300 m. These points were excluded from the analysis.

5. DISTRIBUTION OF SUBDUCTED WATER MASSES

Subducted water masses occur frequently in the CTZ based on the numbers of profiles from each grid survey which contain them (Fig. 4). They are found both in the seaward flowing jet and near shore, and a few are found in offshore waters south of the jet. Beam c and fluorescence anomalies in the layers from these latter profiles were very weak as were all of the layers in the first survey. In the first three surveys from 20 June - 18 July, no layers are found in offshore waters to the north and east of the jet and those farthest offshore during this time are in the jet itself. A different situation is observed during the fourth survey from 21-27 July when subducted layers are found near the offshore boundary of the grid. They are also seaward of the strongest flow in the jet. Over the time period from the third to fourth grid surveys, the orientation of the jet rotated abruptly from offshore flow to along shore flow where it remained constant at least through the end of the fifth survey. The change in orientation coincided with a general relaxation in the wind field at this time (Stanton et al., 1991), a pattern which has been observed previously in the same area (Strub et al., 1991).

Leg 2 of the Thomas Washington survey was designed to sample selectively the seaward flowing jet and is therefore useful for examining the distribution of subducted water masses here. In addition, this survey included some stations outside of the jet for comparison. Application of the criteria developed in Section 4 shows that subducted water masses are found frequently out along the jet axis with the most seaward of these stations lying almost 300 km from Pt. Arena (Fig. 5). A few stations south of Pt. Arena and inshore of the jet are located in an anti-cyclonic eddy (Swenson and Niller, 1991) and also contain subducted water masses.

Profiles from a group of five stations from those identified in Fig. 5 suggest a gradual sinking of phytoplankton layers along

isopycnal surfaces out the jet axis (Fig. 6A). These stations were not occupied sequentially and do not follow any particular water parcel in a Lagrangian sense. Rather, they illustrate where particle layers can be found in different regions of the jet. At the near shore station 46, high levels of fluorescence and beam *c* are observed above 80 db. Radon deficiencies at this station indicate recent gas exchange throughout this depth range (Kadko et al., 1991) even though no surface mixed layer is present. Surface mixed layers in density are apparent only at offshore stations 67 and 33 in the upper 20 db. Out the axis of the jet, beam *c*, fluorescence, and chlorophyll levels are frequently high on and above the 25.8 isopycnal, which deepens from about 23 db at station 46 to 150 db at station 33. Discrete layers around this level are evident (Figures 6C, 6E, and 6F), but are not continuous in profiles from nearby stations. Measurable beam *c* and fluorescence levels are not limited to the depth of the 25.8 isopycnal and above, but exceed 200 dbar in some stations such as 17A (Fig. 6D) and in stations from the five grid surveys of Fig. 4 as well.

Figure 6 suggests that the vertical distribution of phytoplankton layers may be related to the position of isopycnal surfaces. Because of this we use an isopycnal coordinate system in much of the following analysis. In particular, the distributions of properties on two isopycnal surfaces are examined in some detail: (1) the 25.8, which frequently lies within the euphotic zone; and (2) the 26.2, which is generally below the euphotic zone.

Comparison of the distributions of beam *c* and pressure on isopycnal surfaces indicates that the lateral extent of subducted layers may be large. Offshore, where the 25.8 surface is below 120 db, beam *c* $> 0.4 \text{ m}^{-1}$ at stations 33, 34, 72, and 75 (Figures 7A and 7B); the along axis separation of the 33-34 pair and the 72-75 pair is about 50 km while the cross axis dimension of this layer of particles is at least 28 km. The pattern of isopycnal contours of fluorescence (not shown) is very similar to that for beam *c* in Fig. 7A. The highest levels of beam *c* ($c > 0.7 \text{ m}^{-1}$) on the 25.8 isopycnal occur inshore where this surface lies within the euphotic zone (above 50 db based on Fig. 3B) and is consistent with in situ production of phytoplankton. One of these areas where the 25.8 isopycnal is warped upwards is centered on 124.25 W, 38.75 N and results from the combination of the southward jet flow and the strong northward flow due to an anticyclonic eddy (Fig. 11).

On the deeper 26.2 isopycnal the highest levels of beam *c* ($c > 0.5 \text{ m}^{-1}$) are found near shore at depths below 120 db (Figures 8A and 8B), except for the area immediately south of Pt. Arena which is very shallow and reaches above 50 db. Farther offshore and west of 125.5 W, all points having $c > 0.4 \text{ m}^{-1}$ lie below 120 db. Again the pattern of fluorescence on this surface (not

shown) is very similar. We conclude from this that most of the phytoplankton found on the 26.2 isopycnal in the area covered by the survey were not produced in situ where observed, but instead, have been moved vertically and horizontally by subduction and advection processes out of the euphotic zone in their source regions. This suggests that subduction processes play an important role in governing water mass properties on this isopycnal surface. In contrast, in situ production within the survey area may account for much of the phytoplankton on the 25.8 surface near shore with subduction processes being more important offshore.

6. SOURCES OF SUBDUCTED WATER MASSES

The distribution of beam c and fluorescence on isopycnals like the 26.2 indicate that many of the deep phytoplankton layers probably originate in the euphotic zone away from where they are observed. Because isopycnals slope steeply upward toward the coast in the CTZ area, some lie within the euphotic zone near shore, but at much greater depths farther offshore (Figures 7B and 8B). We hypothesize that these inshore areas where the isopycnals rise into the euphotic zone are the major source regions for the phytoplankton and subducted water masses, although some sources probably lie to the north of the area covered by the surveys. Use of the term "source region" for subducted water masses simply means that they were near the surface there.

If the deep phytoplankton layers originate near shore, then the θ -S relationships in the layers found offshore should be similar to those near shore in the euphotic zone if isopycnal and diapycnal mixing rates are not too large and if particle sinking is not important. For purposes of tracing vertical water mass movement, the phytoplankton act as a dye which identifies water masses which have previously been in the euphotic zone. The θ -S characteristics are potentially useful for tracing horizontal movement of these water masses if remote source regions can be unambiguously identified in θ and S. In contrast to θ and S which are conservative away from the mixed layer, beam c and fluorescence levels are likely to change substantially since phytoplankton concentrations are non-conservative over time scales of a few days and levels change due to a variety of processes such as photosynthesis and grazing by zooplankton. Therefore, the usefulness of fluorescence and beam c as vertical water mass tracers will be limited by their effective loss rates.

In the remainder of this section, the θ -S characteristics of subducted water masses are compared with those of potential source regions for two (overlapping) time periods: first, over the entire experimental period including the time when the jet orientation changed rapidly (late July to early August); and second, during the time when the jet orientation was fairly

stable (late June to mid-July). Higher resolution sampling from the Thomas Washington during this latter period allows more detailed inferences to be drawn regarding near shore source regions.

The locus of all θ -S points from the five grid surveys of Fig. 4 which satisfy the subduction criteria of Section 4 cluster into two areas of distinct characteristics (Fig. 9A). Most of the points fall within a σ_θ range 25.9 - 26.6 (Group A) while a second group is clustered between 25.1 - 25.5 (Group B). Most of the points in the second group are found at the offshore stations in Fig. 4D when the jet orientation changed abruptly. The one exception is offshore station 163 (Fig. 4B) from the first Pt. Sur survey which also falls in Group B. The differences in θ -S characteristics of Group B suggest that the subducted layers found offshore, particularly after the jet reorientation, are not derived from the same sources as those found elsewhere.

Subducted water masses corresponding to the main group of points (Group A) in Fig. 9A are probably derived from near shore sources based on comparisons with upper ocean θ -S characteristics in the CTZ area. All θ -S points in the upper 50 db of the water column from each inshore line of the grid surveys are plotted in Fig. 9B along with the envelope of points from the subducted layers shown in Fig. 9A (Group A). The extensive overlap of the Group A θ -S points with points from the inshore lines is consistent with near shore source regions for the subducted water masses. In contrast, very little overlap is found between the Group A subducted layer θ -S points and those from all of the other (offshore) lines from the grid surveys (Fig. 9C). The upper 50 db of the water column is chosen because this range falls within the euphotic zone throughout most of the survey area (Fig. 3). However, this may underestimate the depth range of the euphotic zone in near shore areas since some of the θ -S points in the subducted layers correspond to higher densities than found near shore above 50 db.

It is also likely the majority of the subducted water masses observed within the jet during the process sampling from the Thomas Washington (Fig. 5) result from near shore sources. During this sampling, the position and water mass composition of the jet were fairly constant for about a month covering the period 20 June to 18 July (Huyer et al., 1991). The consistent orientation of the jet may be seen in the first three geopotential anomaly fields of Fig. 4. Most of the θ -S points within the subducted layers of the jet, identified in Fig. 5, fall within the Group A envelope of θ -S points in Fig. 9A. However, a few such as those from Station 35 which is located far offshore, fall within the Group B envelope and may indicate another source farther offshore (Figures 10A and 10B).

The θ -S points for the subducted water masses within the jet are consistent with formation by isopycnal mixing of waters from different near shore source regions. Based on θ -S distributions in the upper 50 db of the water column, two potential source regions are identified: (1) the waters offshore and north of Pt. Arena (and possibly north of the study area), represented by station A3, and (2) waters immediately north of Pt. Reyes, represented by station A13 (Fig. 10B). Points lying between the A3 and A13 curves could be formed by advection and isopycnal mixing of waters from these two source regions. However, source water contributions from the area around Pt. Reyes require a northward coastal flow inshore of the jet. The θ -S curves of Fig. 10B (solid lines) are obtained from leg 1 data of the Thomas Washington survey (25 June - 2 July) and show that waters on the southern end of the inshore line are generally saltier on a given isopycnal than those to the north. This situation persisted during all of the grid surveys based on isopycnal plots of "spiciness" presented by Huyer et al. (1991).

On some isopycnals near shore, a correspondence is observed between flow direction and θ -S properties which is consistent with the hypothesis that the subducted layers originate from at least two inshore source regions. A detailed θ -S diagram containing only points in subducted water masses below 120 db which lie on $\sigma_\theta = 26.2$ (Fig. 10C) shows that θ -S points at stations 9A and 47, in the southward flow of the jet (Fig. 10A), are very similar to those at Station A3 located north of Pt. Arena. The southward flow of the jet at station 47 penetrates to about 300 db and the maximum near surface geostrophic velocity is 0.7 m/s (Fig. 11). Contours of geostrophic velocity (reference level of 500 db) of Fig. 11 are based on a line of stations extending offshore from just south of Pt. Arena (stations 47 - 53 in Fig. 14A). In contrast, at stations 51 and 52, which are in northward flow (Fig. 11), θ -S points are nearly identical to those at Station A13 located just off Pt. Reyes. The remaining points lie between these end members. The combination of northward flow in the center of the line of stations 47 - 53 with southward flow on the east end of the line (Fig. 11) is due the presence of the anticyclonic eddy just inshore of the jet mentioned previously. This eddy is evident in drifter tracks reported by Swenson et al. (1991). A similar pattern of geostrophic velocity is also observed 20 km to the south on the line of stations 57 - 65 (station locations shown in Fig. 14A).

Further evidence that Pt. Reyes may be a source region for some of the subducted layers is the distribution of S on $\sigma_\theta = 26.2$ from legs 1 and 2 of the Thomas Washington survey. Salinities exceeding 33.82 are found on the two lines of stations from leg 2 that extend offshore from just south of Pt. Arena (Fig. 12); these points generally are found below 90 db (Fig. 8B) and have high levels of beam c (Fig. 8A) and fluorescence. Two

of these stations, 51 and 52, satisfy the subduction criteria of Section 4. The high salinity of these waters ($S > 33.82$) is consistent with northward (and downward) advection from the Pt. Reyes area along the 26.2 isopycnal. The more comprehensive inshore survey (leg 1) obtained about 18 days earlier shows that $S > 33.82$ on $\sigma_\theta = 26.2$ at three stations (A11, A12, and A13) near Pt. Reyes, but nowhere to the north (Fig. 13A). Clearly, considerable evolution of the near shore salinity field occurred over this time period. Northwestward advection of high salinity water along $\sigma_\theta = 26.2$ from the vicinity of Pt. Reyes would require an average speed of about 0.07 m/s to account for the changes in S near Pt. Arena. This estimate falls well within the range of northward geostrophic velocities on the 26.2 isopycnal along the line of stations 47 - 53 (Fig. 11).

Not only is the salinity distribution consistent with the idea that Pt Reyes is a subduction source region, but so are the distributions of beam c , fluorescence, and pressure on $\sigma_\theta = 26.2$. In the waters off Pt. Reyes, the 26.2 isopycnal reaches vertically to within about 40 db of the surface (ie. within the euphotic zone) at station A13 (Fig. 13B) and has $c > 0.8 \text{ m}^{-1}$ (Fig. 13C). High levels of beam c at pressures of about 90 db and less are evident at stations A11, A12, and 13. The fluorescence contours (not shown) are very similar to the beam c contours here. Thus, waters found near Pt. Arena below 120 db, such as stations 51 and 52, may originate in the near the surface waters off Pt. Reyes where similar S , beam c , and fluorescence characteristics are found.

7. VERTICAL TRANSPORT BY ISOPYCNAL SINKING

One mechanism that could result in vertical movement of water masses out of the euphotic zone and subsequent transport offshore to depths exceeding 120 db is simply flow along sloping isopycnal surfaces out the axis of the jet. Evidence for water mass sinking in the jet comes from a sequence of CTD stations made daily alongside a surface drifter (path shown with solid line in Fig. 14A). Averages of densities in the upper 10 m of the water column progressively decrease and the total change from the beginning to the end of the track is about 0.7 kg/m^3 . Fluid particles traveling on the 25.8 or 26.2 isopycnal surfaces could experience depth changes of well over 100 m based on the distributions of pressure of these surfaces (Figures 7B and 8B). A particle moving on a density surface would probably not change depth monotonically because local depth variations result from processes like mesoscale eddy activity.

The time required for a water particle to move out the jet axis on a particular isopycnal varies greatly because of strong vertical shear in the jet. Depending upon the mean advective speed and the depth of a particular isopycnal, the time scale for this process to occur ranges from a few days to a few weeks.

This advective time scale is of interest because it puts a lower bound on the persistence time for the subduction indicators used in this analysis (beam c and fluorescence) and it gives an estimate of the order of magnitude of typical vertical velocities. To illustrate how this isopycnal sinking out of the euphotic zone might proceed, the advection times and vertical and horizontal velocities are computed along hypothetical drifter tracks located on the 25.8 and 26.2 isopycnal surfaces.

Advective time scales for flow along these isopycnals are estimated from 8 sections of geostrophic velocity which cross the jet at approximately right angles to the flow (Fig. 14A). The sections were obtained over a two week period (7 - 21 July) during the time when the position of the jet was relatively constant (Huyer et al. 1991). Geostrophic velocity profiles are computed from adjacent pairs of stations on these transects and use a reference level of 500 db. Some sections show sloping density surfaces down to 500 db so actual velocities may be larger. Geostrophic velocities are then interpolated onto the isopycnals based on the average pressure of the given isopycnal for each pair of stations; examples of isopycnal velocity profiles on $\sigma_\theta = 26.2$ are shown in Figures 14B to 14E. Negative velocities indicate generally southward or offshore flow and the shapes of the profiles are approximated by polynomial fits to data points from station pairs.

On the two inshore lines 47 - 53 and 65 - 57, a region of strong cyclonic vorticity separates the southward flowing jet from the northward flow of the anti-cyclonic eddy (Fig. 14B and 14C). The region of southward flow in the eddy is barely resolved on the east end of each line. Farther out the jet along the line of stations 17A - 21, the flow field exhibits lower vorticity and is offshore everywhere in the profile (Fig. 14D). The mean velocity from this profile is -0.14 m/s. The offshore flow of the jet is still detectable at the most offshore line 73 - 76, 360 km from shore, and shows lower vorticity with a mean velocity of -0.11 m/s.

Advective time and velocity scales along the hypothetical drifter tracks at three levels in the jet are summarized in Table 1. Mean velocity and time scales are based on averages of only the portions of each profile which are in the jet (southward or offshore flow); eddy or recirculating portions of isopycnal velocity profiles are not included in the means. The minimum time scales and maximum velocity scales are based on the maximum jet velocity in each section. We take minimum transit times and maximum velocities to be more representative of the jet axis while the maximum times and minimum velocities are representative of off axis conditions. The end points for the hypothetical drifter tracks are stations 48 and 75 and the track length is 321 km (dotted line, Fig. 14A). The hypothetical drifter on the 25.8 isopycnal begins at about 20 db at station 48, well within the euphotic zone, and requires from 12 to 21 days to reach station

75 where it would be at about 140 db. The corresponding times on the 26.2 surface are about double these times while those at 5 db are about half. For comparison, the track of an actual surface drifter is also shown in Figure 14A (solid line). This drifter took 5.1 days to travel from station 6 to station 32 which compares favorably with minimum and mean times (between stations 48 and 32A) of 4.5 - 9.8 days using the geostrophic velocities at 5 db/500 db in the cross-jet sections of Fig. 14A.

8. DISCUSSION AND CONCLUSIONS

Shipboard CTD and bio-optical observations made during the summer upwelling season in 1988 reveal the presence of deep phytoplankton layers below the euphotic zone in many areas of the coastal transition zone (CTZ), including a strong baroclinic jet which was present throughout the observational period. A principal conclusion of this study is that the water masses associated with the phytoplankton have been moved downward by subduction processes. This finding is supported by the distributions of several hydrographic and geochemical tracers, including ^{222}Rn , chlorophyll, and dissolved oxygen (Kadko, et al. 1991). Criteria to objectively identify subducted water masses have been developed and are based on the light field in the water column and levels of chlorophyll fluorescence and the beam attenuation coefficient (beam c). Subducted water masses are observed in all six hydrographic grid surveys of the CTZ experiment which covered the period 20 June - 4 August, 1988.

The θ -S relationships corresponding to the subducted water masses fall into two distinct groups and are consistent with two near surface subduction regions, one near shore and a second much farther offshore. The scatter in θ -S points suggests that the near shore source is distributed along shore and has contributions from the area in the vicinity of Pt. Reyes and from an area north of Pt. Arena, or possibly north of the study area. Subducted water masses from the near shore source region were present throughout the experimental period, while those from the offshore source were most frequently observed just after the strong baroclinic jet changed orientation from offshore to alongshore flow.

The positions of layers of phytoplankton in the water column indicate that some water masses sink over 100 m as they are advected out along the jet axis. Similar, but much larger, vertical displacements resulting from isopycnal advection in a strong, meandering baroclinic jet (the Gulf Stream) have been observed in RAFOS float trajectories by Bower and Rossby (1989). Vertical displacements could also result from mixing processes acting along sloping isopycnals, both along and across the jet axis. Vertical advection rates based on geostrophic flow on sloping density surfaces are 6-10 m/day for the 25.8 surface and

2-4 m/day for the deeper 26.2 surface. These estimates are averages based on advection over 320 km of the jet axis and probably underestimate maximum vertical velocities. This is because isopycnals rise up into higher velocity flow near shore where isopycnal slopes are generally the largest. Kadko et al. (1991) estimate vertical velocities as high as 27 m/day based on ^{222}Rn deficiencies. Advective time timescales out the jet are about 2 - 3 weeks along the 25.8 isopycnal and about double this along the 26.2 isopycnal. This indicates that detectable levels of beam c and fluorescence from subducted phytoplankton can persist for several weeks.

A variety of other physical processes may lead to water mass subduction and not all of them are associated with the jet since subducted layers are found at several stations outside of the jet (Figures 5 and 6). Drifter observations of Brink et al. (1991) show that convergence zones exist offshore in the jet with associated downwelling velocities of order 10 m/day. Vertical velocities of order 20 m/day and larger which result from changes in relative vorticity are reported by Swenson et al. (1991) from clusters of drifters deployed in the jet. Persistent vertical velocities of this same magnitude are found in the vorticity and vertical velocity analysis of Dewey et al (1991). Another mechanism that could lead to water mass subduction is the interaction of the jet with a large scale deformation field. The resulting ageostrophic, cross jet transport leads to downwelling on the cyclonic side of flank of the jet (Onken et al, 1990). Numerical modeling experiments for the CTZ area also result in downward vertical velocities consistent with our observations (Hoffman, et al., 1991)

Two important issues concerning the impact of subduction processes on the circulation in this coastal transition zone are the total volume of subducted water and the vertical volume flux. A lower bound on the subducted volume in the jet may be estimated by assuming that the fraction of all profiles in the jet satisfying the subduction criteria developed in Section 4 is representative of the jet volume as a whole. During Leg 2 of the Washington cruise, a total of 50 profiles were obtained in the jet (ie. 5/500 db dynamic height in the range 0.82 to 0.96 m) and just over 1% of all the water column from these profiles satisfy the criteria. The total volume of the jet above 500 m in the survey area is about 9000 km³ so the subducted volume is of order 100 km³. Assuming that the total subducted volume is transported out the jet axis in 12 to 21 days (the transit times on the 25.8 isopycnal from Table 1) and that a steady state volume of subducted water is maintained in the jet, the required vertical volume flux is of order 5 to 8 km³/day. An estimate of the vertical mass flux of chlorophyll may be made using the average fluorescence level in the subducted layers and a chlorophyll calibration derived for the depth range from the 1% light level to 150 m (separate analysis by one of the authors, BHJ). The

mean chlorophyll concentration is about $1 \mu\text{g}/\text{l}$ and the resulting vertical mass flux of chlorophyll is of order of $(5 - 9) \times 10^3 \text{ kg}/\text{day}$.

The subducted volume estimate of 100 km^3 is likely an underestimate for the study area as a whole, possibly by as much as an order of magnitude, for two reasons. First, the depth criteria of 120 m is very conservative since it is based on the deepest 0.1% light level in the clearest offshore waters. If this criteria is relaxed to say the average 0.1% light level found in the jet, about 83 m, then the fraction of the water column satisfying the subduction criteria would be 4 times larger based on Fig. 3C. (This average 0.1% light level is based on analysis, not presented here, by one of the authors, BHJ.) Second, only about one third of the stations from all of the grid surveys showing evidence of subduction is found in the jet (Fig. 5). Combining these factors, the total subducted volume in the entire study area may be as large as 1000 km^3 and, if the vertical processes leading to subduction have similar rates inside and outside the jet, the vertical volume flux might be as much as $80 \text{ km}^3/\text{day}$. The corresponding vertical mass flux of chlorophyll in this case would be of order $9 \times 10^4 \text{ kg}/\text{day}$. For illustration, the areas of a 50 m deep euphotic zone which would be subducted by vertical volume fluxes of 5 and $80 \text{ km}^3/\text{day}$ are indicated by squares in Fig. 5. The larger square is 40 km on a side. Clearly, more observations are required to constrain the subducted volumes and rates and to determine the impacts of subduction processes on coastal circulation and ecology.

ACKNOWLEDGEMENTS

Ken Brink and Dave Mackas provided helpful comments on an early draft of the manuscript. This work was supported by the Office of Naval Research, Coastal Sciences Program.

REFERENCES

- Anderson, G.G., 1969, Subsurface chlorophyll maximum in the Northeast Pacific Ocean, *Limnol. Oceanogr.*, 14, 386-391.
- Baker, E.T., and J.W. Lavelle, 1984, The effect of particle size on the light attenuation coefficient of natural suspension, *J. Geophys. Res.*, 89, C5, 8197-8203.
- Beers, J.R., F.M.H. Reid, and G.L. Stewart, 1975, Microplankton of the NORTH Pacific central gyre. Population structure and abundance, June 1973, *Int. Rev. Gesamten Hydrobiol.*, 60, 607-638.

- Bienfang, P., J. Szyper, and E. Laws, 1982, Sinking rate and pigment responses to light-limitation of a marine diatom: implications to dynamics of chlorophyll maximum layers, *Oceanol. Acta*, 6, 1, 55-62.
- Bienfang, P., and J. Szyper, 1982, Effects of temperature and salinity on sinking rates of the centric diatom *Ditylum Brightwelli*, *Bio. Oceanogr.*, 1, 3, 211-223.
- Bienfang, P.K., 1981, Sinking rate dynamics of *Cricosphaera Carterae* Braarud. 1. Effects of growth rate, limiting substrate, and diurnal variations in steady-state populations, *J. Exp. Mar. Ecol.*, 49, 217-233.
- Bishop, J.K.B., 1986, The correction and suspended particulate matter calibration of Sea Tech transmissometer data, *Deep-Sea Res.*, 33, 1, 121-134.
- Bower, A.S., and T. Rossby, 1989, Evidence of cross-frontal exchange processes in the Gulf Stream based on isopycnal RAFOS float data, *J. Phys. Oceanogr.*, 19, 9, 1177-1190.
- Brink, K.H., R.C. Beardsley, P.P. Niiler, M. Abbott, A. Huyer, S. Ramp, T. Stanton, and D. Stuart, 1991, Statistical properties of near surface flow in the California coastal transition zone, *J. Geophys. Res.*, (submitted).
- Cullen, J.J., 1982, The deep chlorophyll maximum: comparing vertical profiles of chlorophyll a, *Canadian J. of Fisheries and Aquatic Sci.*, 39, 791-803.
- Davis, R.E., 1985. Drifter observations of coastal surface currents during CODE: the statistical and dynamical views, *J. Geophys. Res.*, 90, 4756-4772.
- Dewey, R.K., J.N. Moum, C.A. Paulson, D.R. Caldwell, and S.D. Pierce, 1991, Structure and dynamics of a coastal filament, *J. Geophys. Res.*, (submitted).
- Flament, P.J., A. Armi, and L. Washburn, 1985, The evolving structure of an upwelling filament, *J. Geophys. Res.*, 90, 11,765-11,778.
- Hoffman, E.E., K.S. Hedstrom, J.R. Moisan, D.B. Haidvogel, and D.L. Mackas, The use of simulated drifter tracks to investigate general transport patterns and residence times in the Coastal Transition Zone, *J. Geophys. Res.*, submitted.
- Hood, R., 1990, Phytoplankton biomass, photosynthetic light response, and physical structure in a Northern California upwelling system, Ph.D. dissertation, Scripps Institution of Oceanography.
- Huyer, A., F. Chavez, T. Cowles, J. Fleischbein, P.M. Kosro, S.

Jackson, G., 1991, A model of formation of marine algal flocs by physical coagulation processes, in press, Deep-Sea Res.

Jerlov, H.G., 1976, Marine Optics, Elsevier, New York, 231 pp.

Kadko, D.C., L. Washburn, and B.H. Jones, 1991, Evidence of subduction within cold filaments of the N. California coastal transition zone, submitted, J. Geophys. Res.

Kiefer, D.A., 1973, Fluorescence properties of natural phytoplankton populations, Mar. Bio., 22, 263-269.

Onken, R., J. Fischer, and J.D. Woods, Thermohaline finestructure and its relation to frontogenesis dynamics, J. Phys. Oceanogr., 20, 9, 1379-1394.

Pak, H., J.R.V. Zaneveld, 1977, Bottom nepheloid layers and bottom mixed layers observed on the continental shelf off Oregon during the upwelling season, J. Geophys. Res., 82, 3921-3931.

Prezelin, B.B., 1981, Light reactions in photosynthesis, Physiological bases of phytoplankton ecology, Canadian Bulletin of Fisheries and Aquatic Sci. (T. Platt, Ed.), 210, 1-43.

Smayda, T.J., 1970, The suspension and sinking of phytoplankton in the sea, Oceanogr. Mar. Biol. Ann. Rev., 8, 353-414.

Smetacek, V.S., 1985, Role of sinking in diatom life-history cycles: ecological, evolutionary, and geological significance, Mar. Bio., 84, 239-251.

Spinrad, R.W., 1986, A calibration diagram of specific beam attenuation, J. Geophys. Res., 91, C6, 7761-7764.

Stanton, T.P., J. Stockel, M.L. Batteen and S. Ramp, 1991, Upper ocean response to a wind relaxation event in the coastal transition zone, submitted to J. Geophys. Res.

Strub, P.T. and the CTZ Group, 1991, The nature of the cold filaments in the California Current System, submitted to J. Geophys. Res.

Swenson, M., P.P. Niiler and K. Brink, 1991, The dynamical and thermodynamical structure of the flow associated with a cold filament off Pt. Arena, California in July 1988, submitted to J. Geophys. Res.

Table 1. Advection times and velocities along jet*

Level	Time (days)	Horizontal Velocity (m/s)	Vertical Velocity (m/s)
	Min. - Mean	Max. - Mean	Max. - Mean
5 db	5 - 11	0.70 - 0.33	
$\sigma_\theta = 25.8$	12 - 21	0.30 - 0.17	10 - 6
$\sigma_\theta = 26.2$	20 - 42	0.18 - 0.09	4 - 2

*Stations: 48-62-88-19-26-39-32A-75
 Total distance = 321 km

FIGURE CAPTIONS

Fig. 1A. Locations of stations E4 and 6. Contours of geopotential anomaly (0/500 db) are from first Pt. Sur survey, 6 - 12 July 1988.

Fig. 1B. Profiles of photosynthetically available radiation (PAR), beam c, and fluorescence at station 6 along with chlorophyll concentrations at discrete depths from bottle samples.

Fig. 1C. Profiles of potential temperature, potential density, and salinity at station 6.

Fig. 2A. As in 1B, but for station E4.

Fig. 2B. As in 1C, but for station E4.

Fig. 3A. Location of PAR profiles obtained within one hour of local noon (triangles). Contours of geopotential anomaly (0/500 db) are from first Pt. Sur survey, 6 - 12 July 1988. Offshore extension of geopotential anomaly contours from leg2 of Thomas Washington survey.

Fig. 3B. PAR profiles obtained within one hour of local noon in: the offshore jet (solid lines), southern and inshore waters (dotted lines), and offshore waters (dashed lines). Vertical bar shows range in 1% light level in jet. Arrows indicate depths of 1% and 0.1% light levels in clear offshore waters.

Fig. 3C. Histogram showing distribution of fluorescence in water column from all CTD profiles obtained during leg 2 of Thomas Washington survey.

Fig. 4. Locations of stations containing subducted water masses shown with filled triangles. Dots show other station locations. (A) first Wecoma survey, 20-27 July; (B) first Pt. Sur survey, 6-12 July; (C) second Pt. Sur survey, 12-18 July; (D) third Pt. Sur survey, 21-27 July; (E) and second Wecoma survey, 29 July - 4 August. Contours of geopotential anomaly (0/500 db).

Fig. 5. Locations of all stations during leg 2 of Thomas Washington survey (triangles). Filled triangles indicate stations with subducted water masses. Contours of geopotential anomaly (0/500 db) are from first Pt. Sur survey, 6 - 12 July 1988. Offshore extension of geopotential anomaly contours from Thomas Washington survey.

Fig. 6A. Locations of profiles in jet shown in Figures 6B to 6F.

Fig. 6B. - 6F. Profiles of potential density, beam c, and fluorescence at five stations along jet axis. Diamonds indicate chlorophyll concentrations from bottle samples.

Fig. 7A. Contour section of beam c on $\sigma_\theta = 25.8$. The x's show station locations.

Fig. 7B. Contour section of pressure on $\sigma_\theta = 25.8$. The x's show station locations.

Fig. 8A. Contour section of beam c on $\sigma_\theta = 26.2$. The x's show station locations.

Fig. 8B. Contour section of pressure on $\sigma_\theta = 26.2$. The x's show station locations.

Fig. 9A. θ -S points corresponding to subducted water masses from the five grid surveys of Fig. 4. Water masses of points in Group A are from near shore sources and Group B from offshore sources.

Fig. 9B. θ -S points in upper 50 db of water column for the most inshore line of the five grid surveys of Fig. 4. Envelope of θ -S points of subducted water masses in Group A (Fig. 9A) shown by dashed lines.

Fig. 9C. θ -S points in upper 50 db of water column for the offshore lines of the five grid surveys. Envelope of θ -S points of subducted water masses (Fig. 9A) shown by dashed lines.

Fig. 10A. Locations of various stations whose θ -S relationships are shown in Figures 10B and 10C.

Fig. 10B. θ -S profiles shown with solid lines are for the stations on line A from leg 1 of the Thomas Washington survey. θ -S points shown with open circles are for subducted water masses observed below 120 db from leg 2 of the Thomas Washington survey. Station locations shown in Fig. 10A.

Fig. 10C. θ -S points of subducted water masses on $\sigma_\theta = 26.2$ and θ -S profiles for the upper 50 db of the water column at stations A3 and A13 (solid lines). Station locations shown in Fig. 10A.

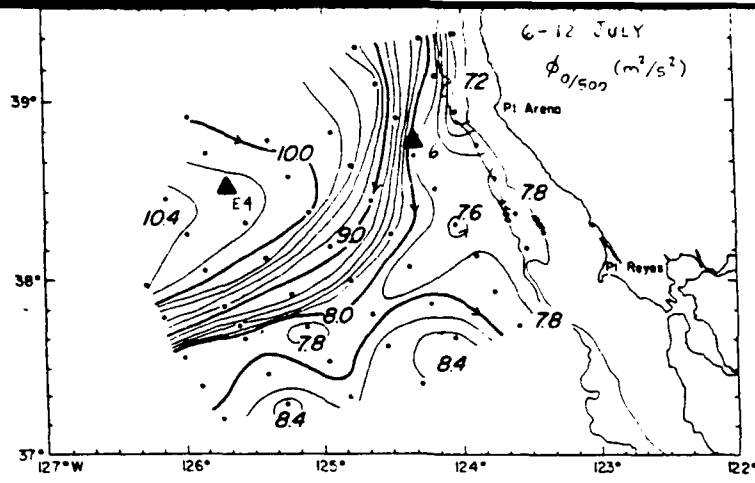
Fig. 11. Vertical section of geostrophic velocity (5/500 db) computed from stations 47 - 53. Station locations shown in Fig. 14A. Stippled areas indicate flow to the south. Dashed line shows position of $\sigma_\theta = 26.2$.

Fig. 12. Horizontal contour section of salinity on $\sigma_\theta = 26.2$ from leg 2 of Thomas Washington survey. Station locations

Fig. 13. Horizontal contour sections on $\sigma_\theta = 26.2$ from leg 1 of Thomas Washington survey of: A. salinity, B. pressure, C. beam c. Station locations indicated with x's.

Fig. 14 A. Cross-jet transects used for computing sections of geostrophic velocity. Track of surface drifter indicated with solid line and hypothetical drifter track with dotted line.

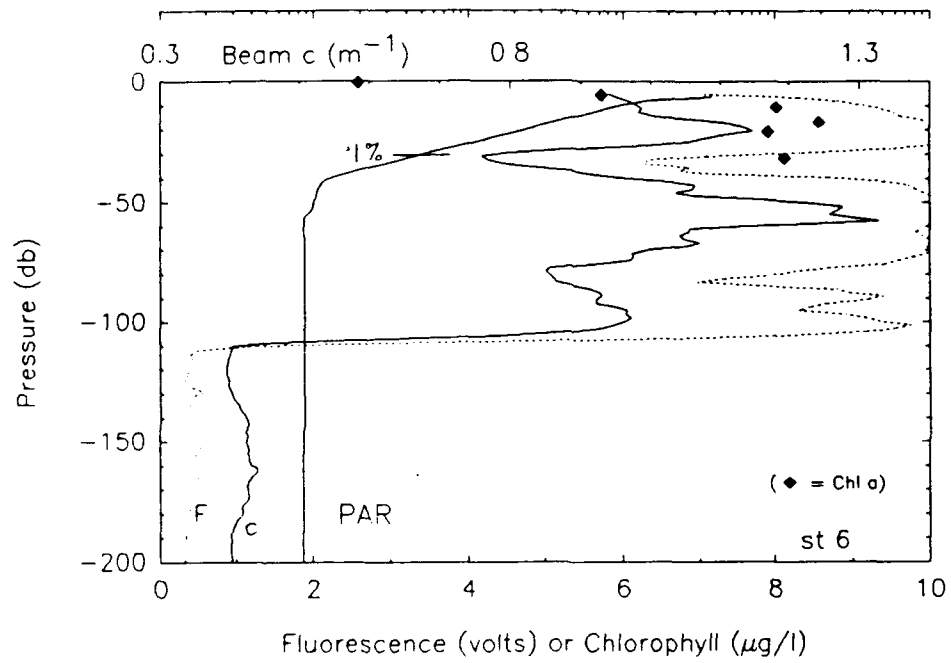
Fig. 14B. - 14E. Isopycnal profiles of geostrophic velocity on $\sigma_\theta = 26.2$ for: (B) stations 47 - 53, (C) stations 65 - 57, (D) stations 17A - 21, and (E) stations 76 - 73.



A.

PAR (quanta/cm²-s)

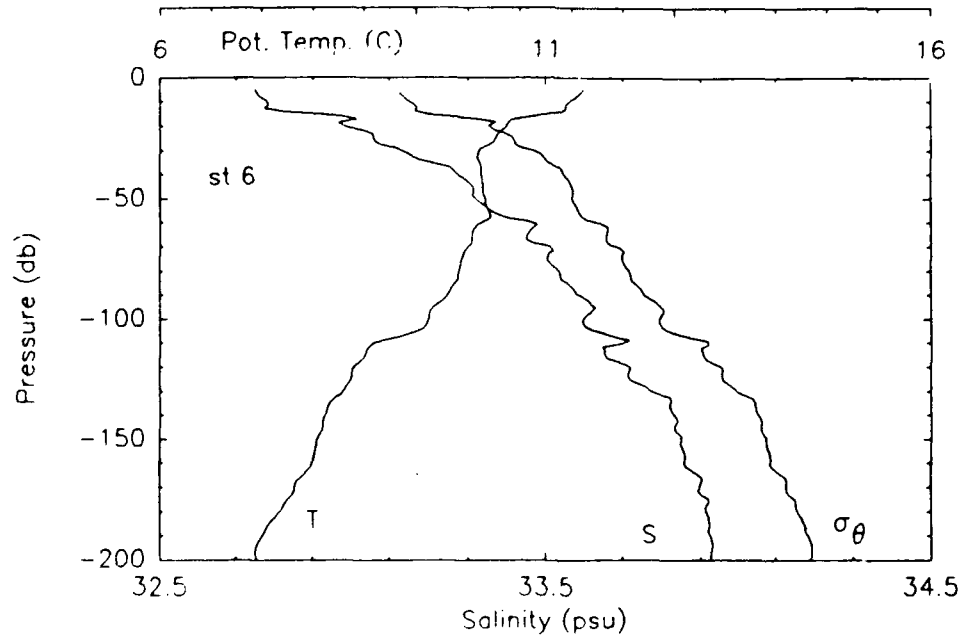
1E13 1E14 1E15 1E16 1E17 1E18



B.

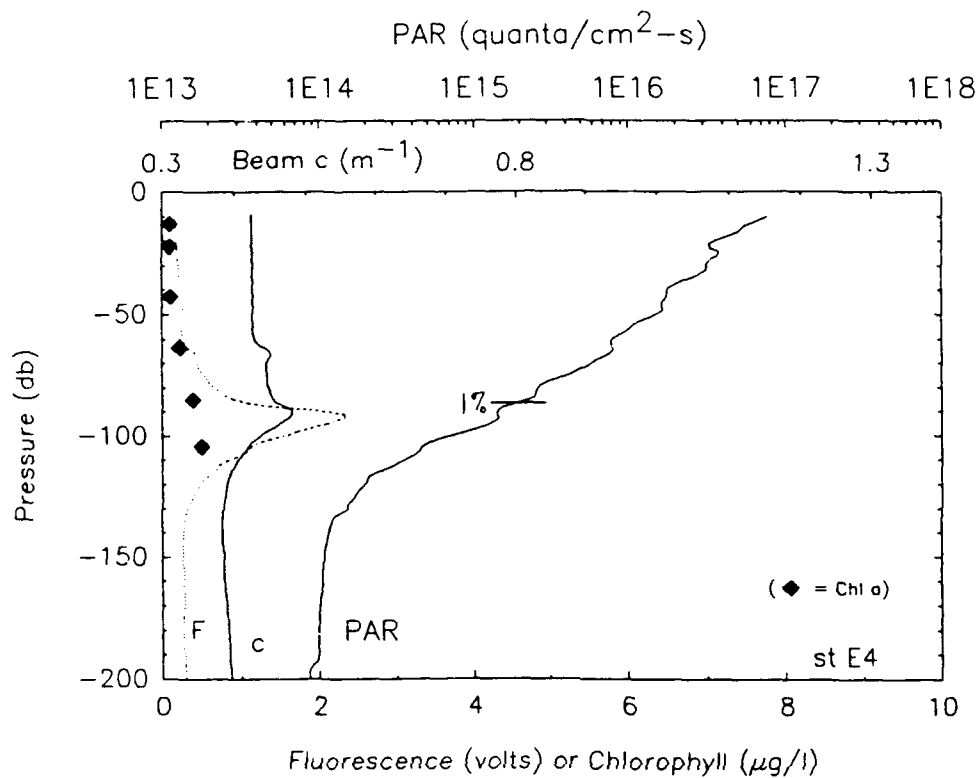
σ_{θ} (kg/m^3)

24 25 26 27



C.

FIG. 1



A.

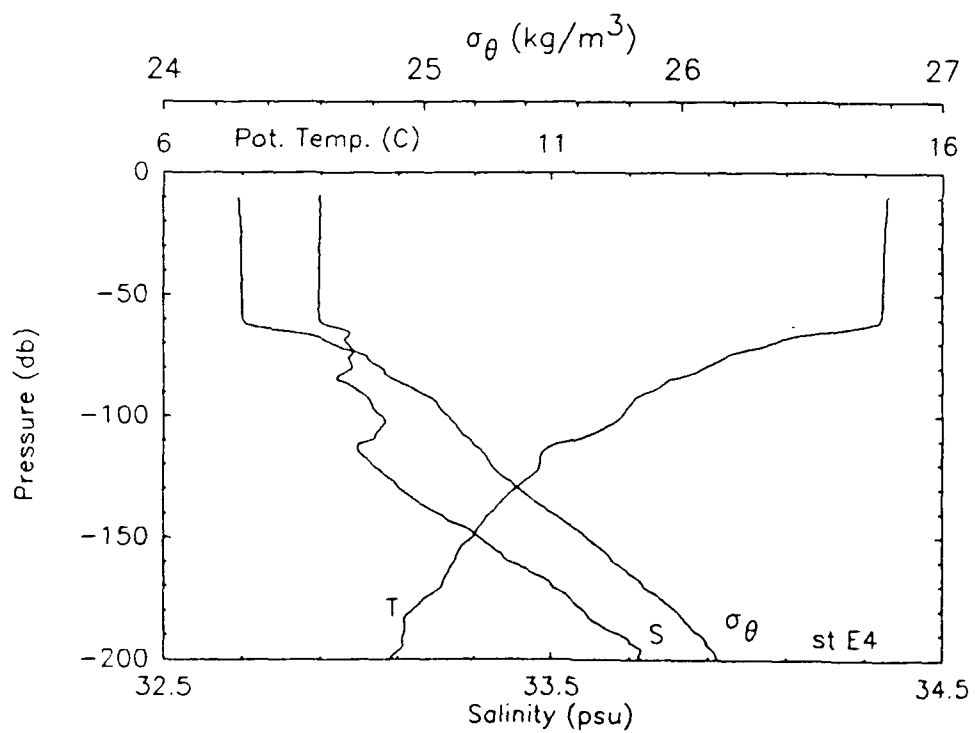
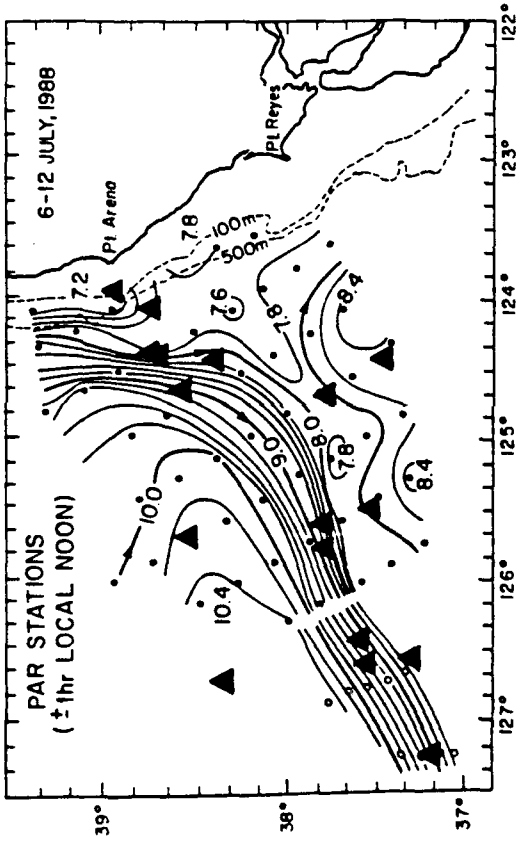


FIG. 2

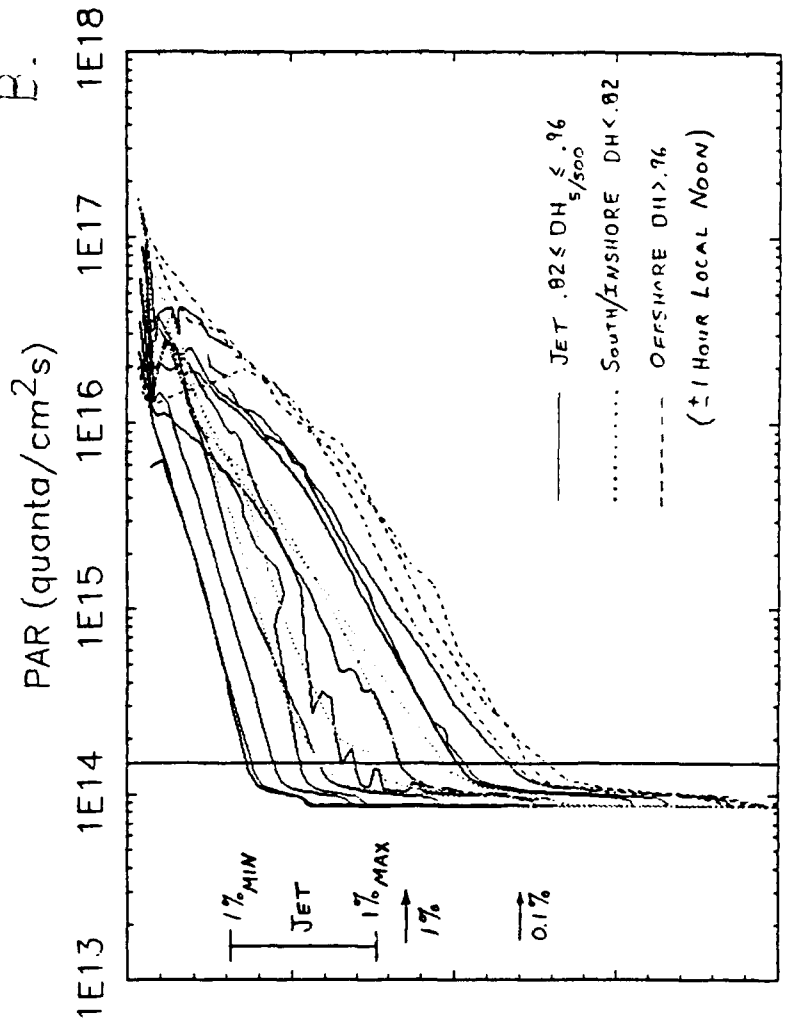
B.

Fig. 3

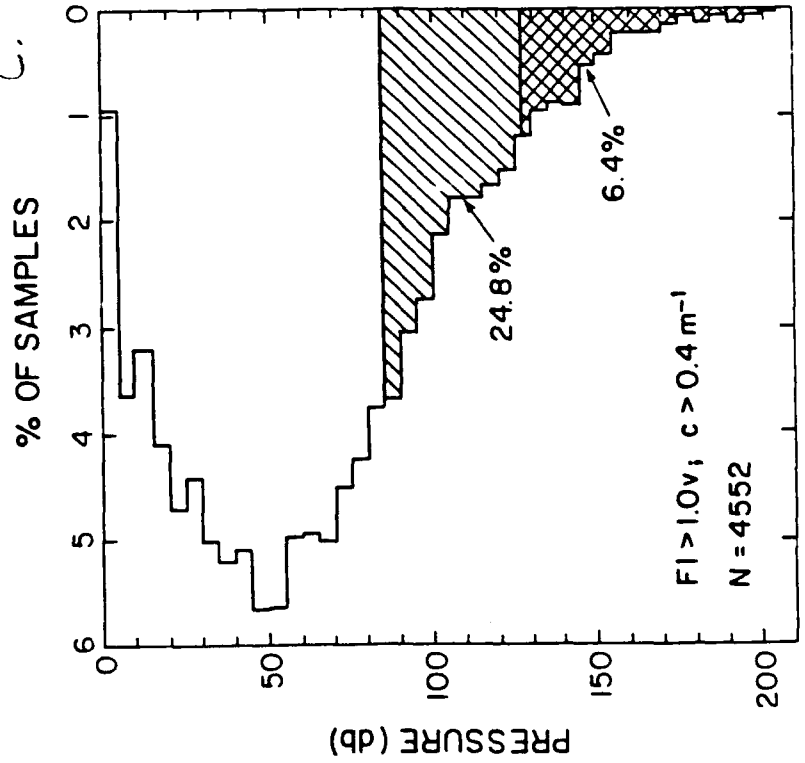
A.



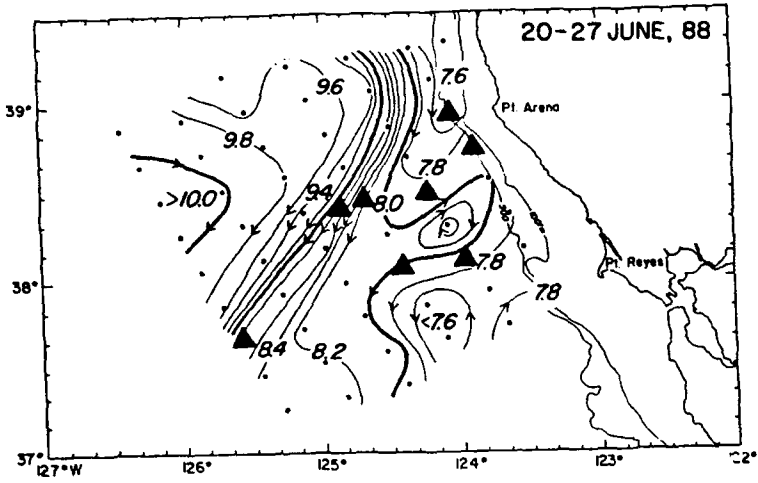
B.



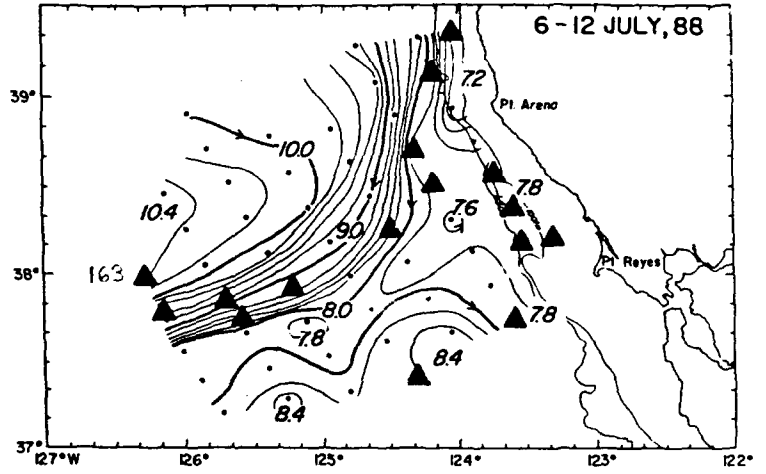
C.



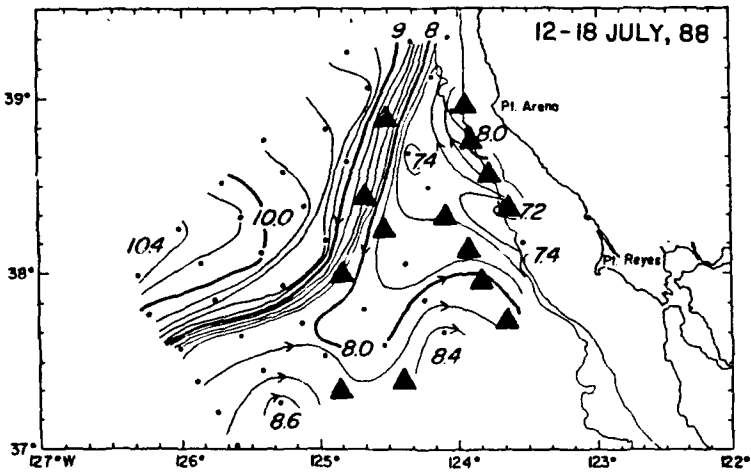
A.



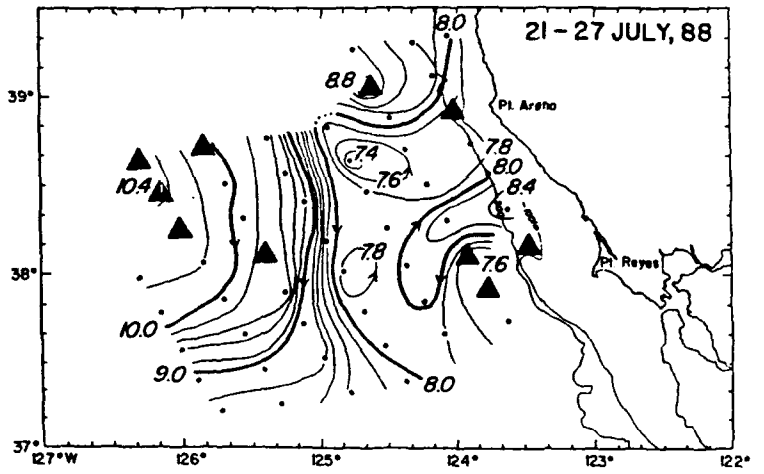
E.



C.



D.



E.

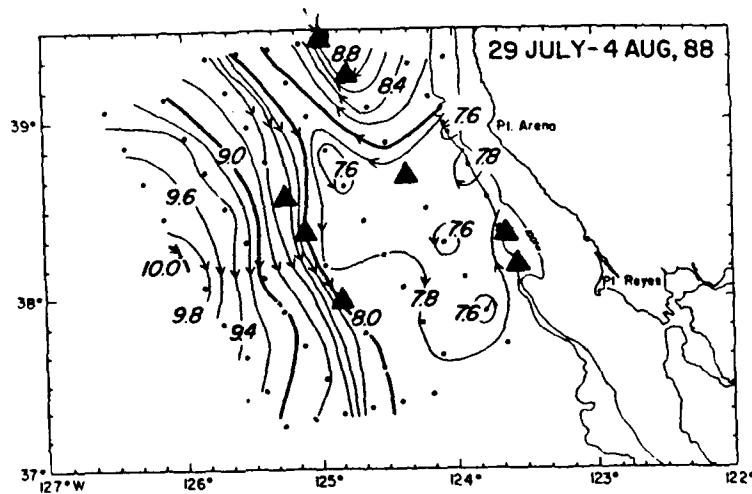


FIG. 4

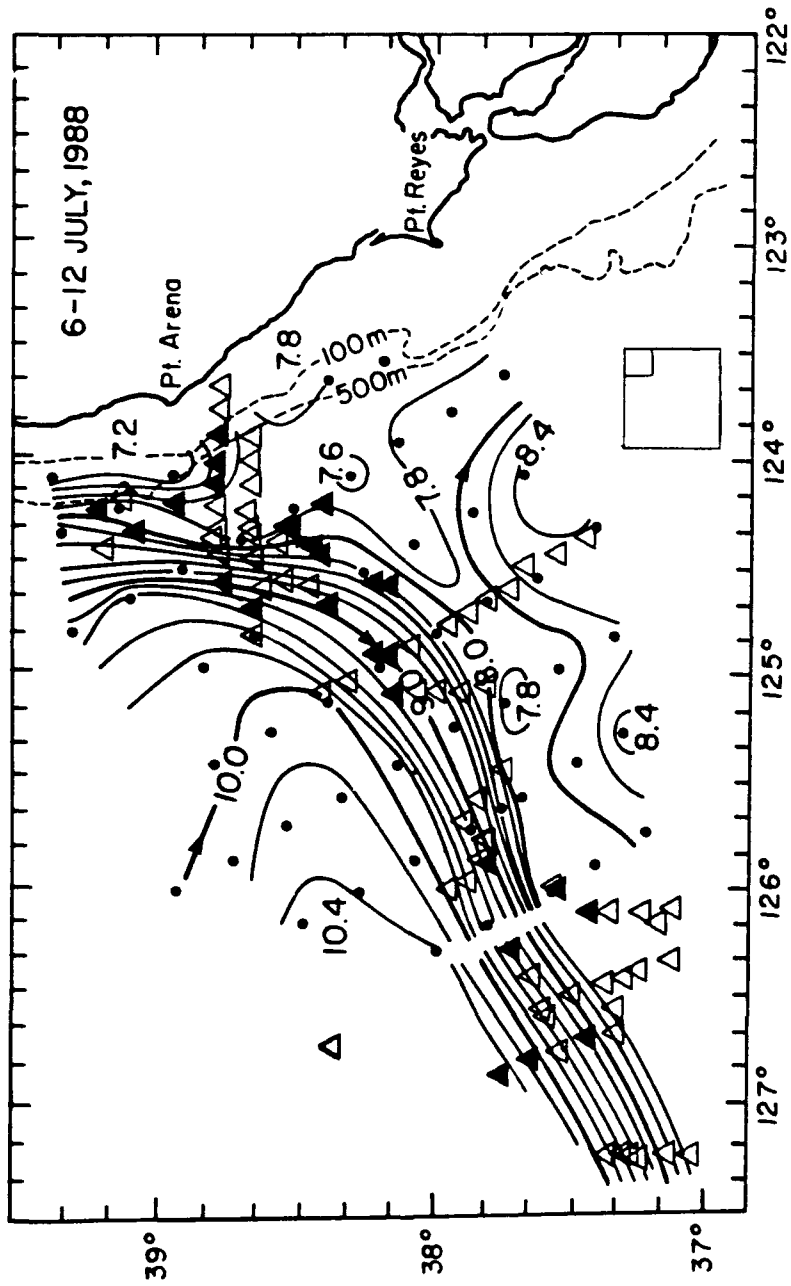


Fig. 5

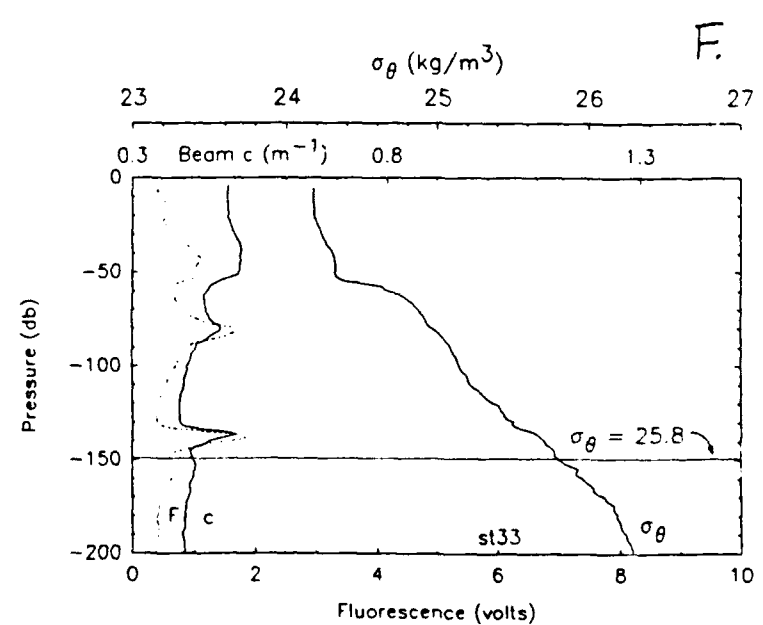
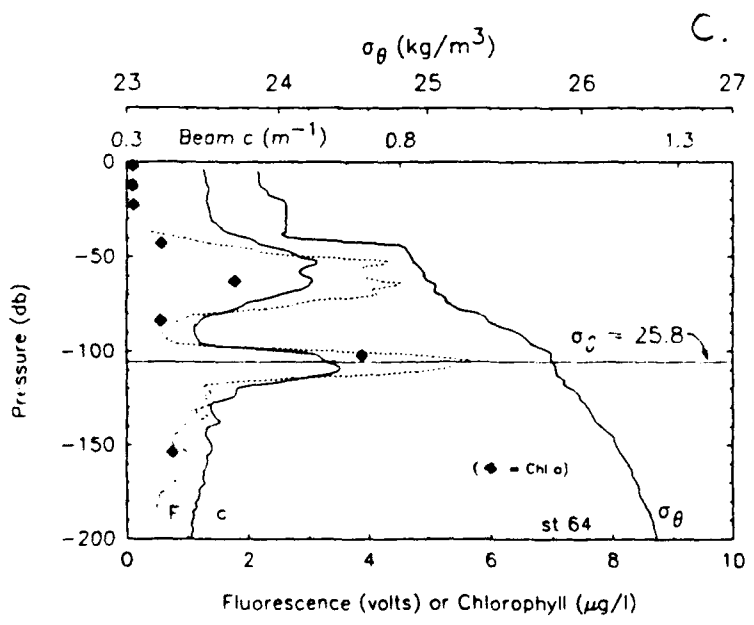
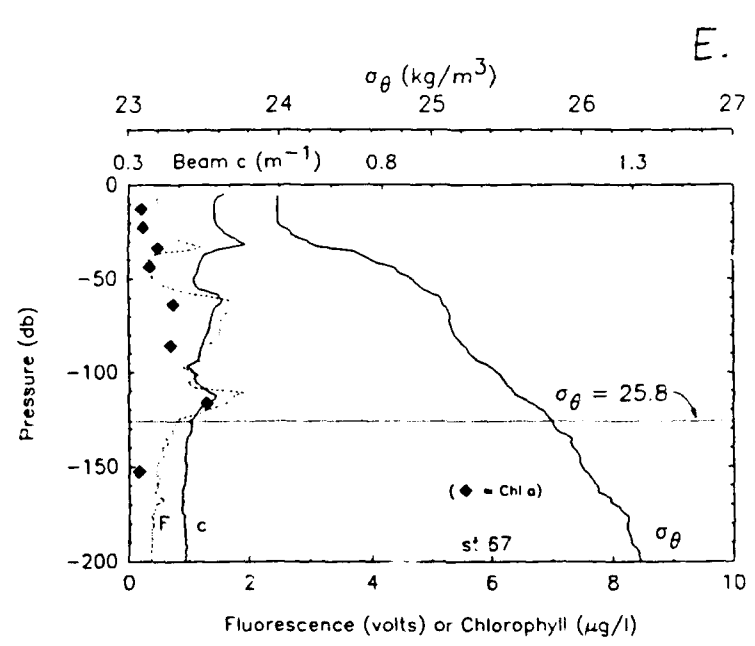
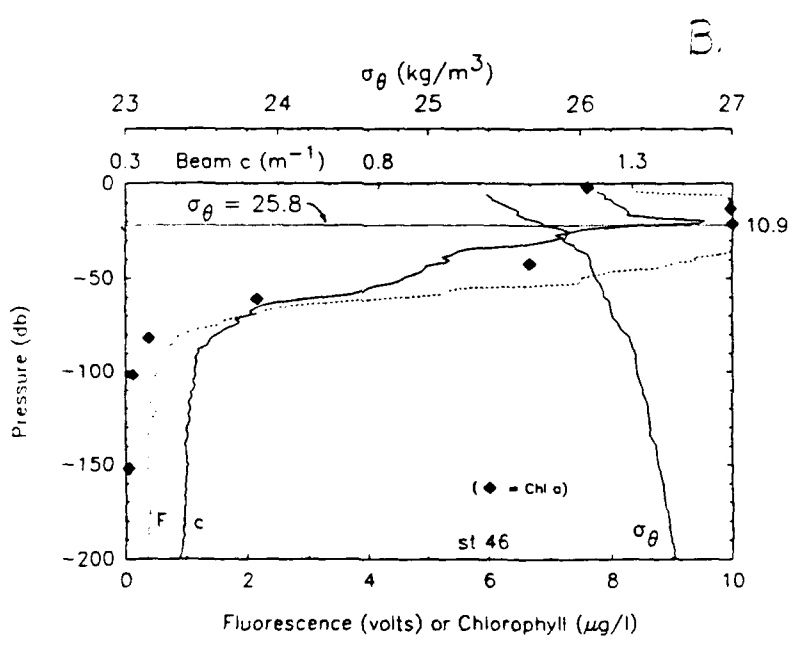
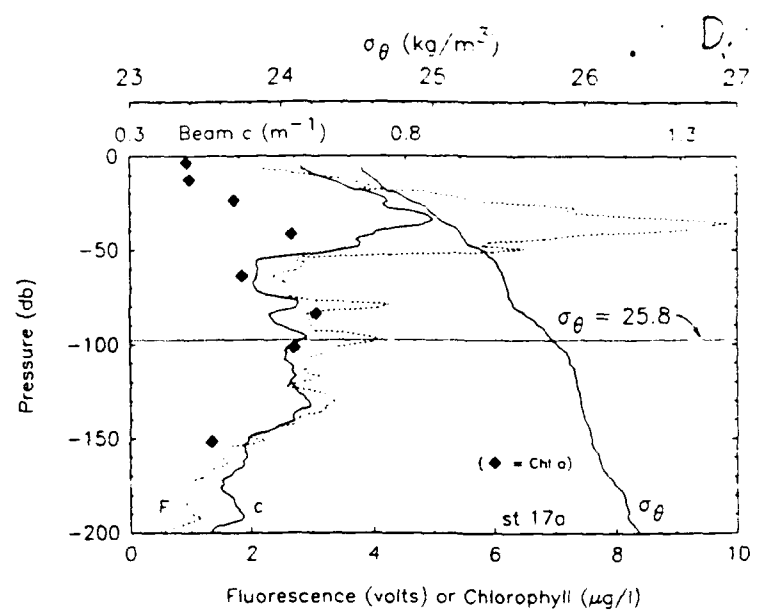
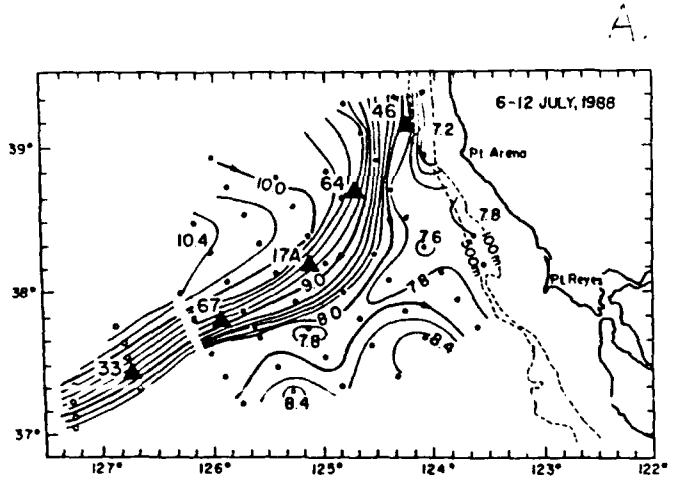
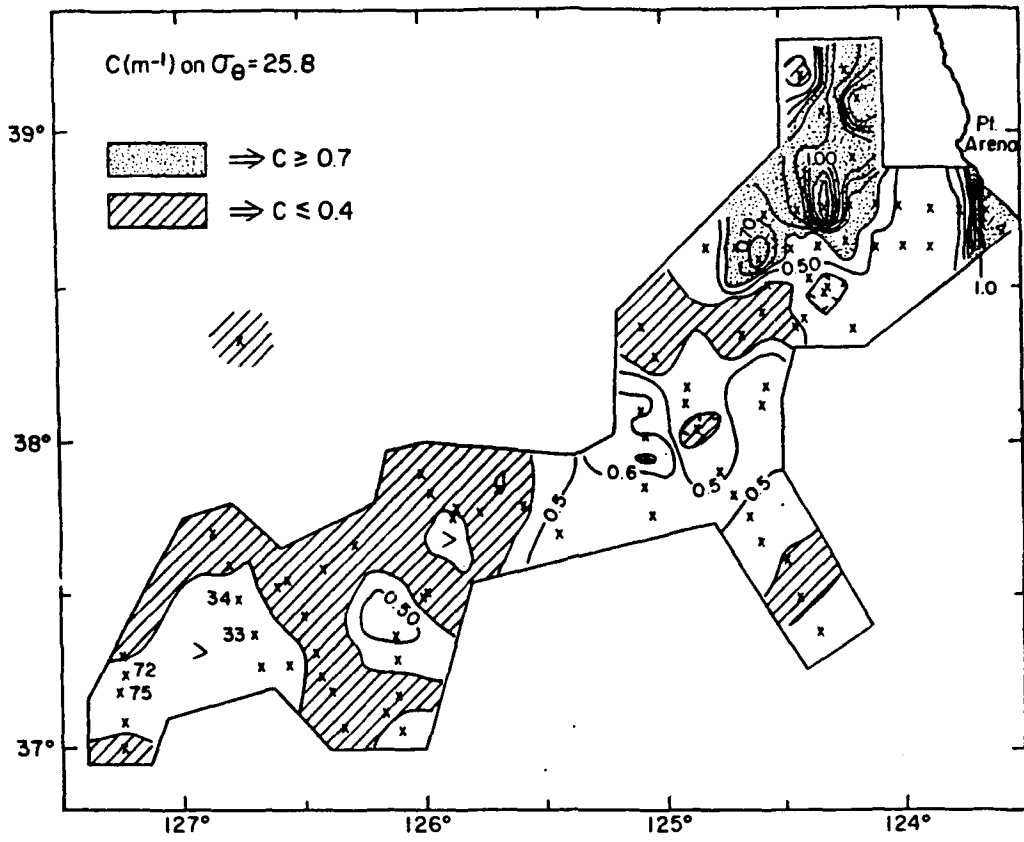
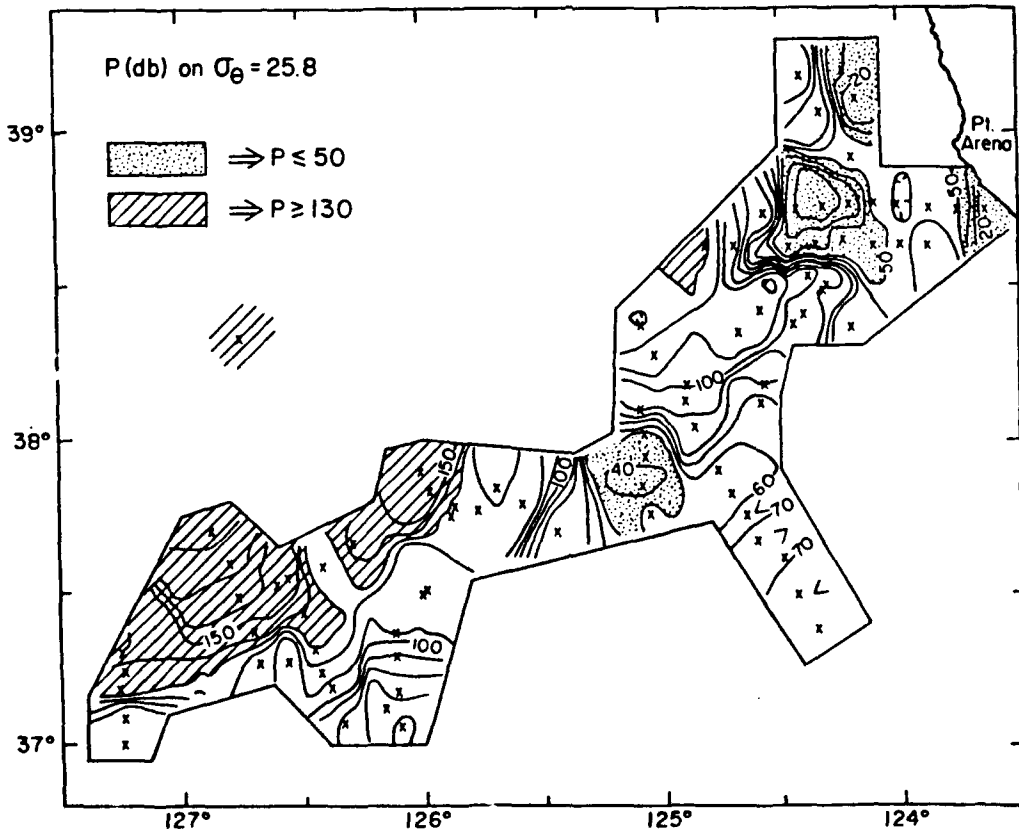


FIG. 6

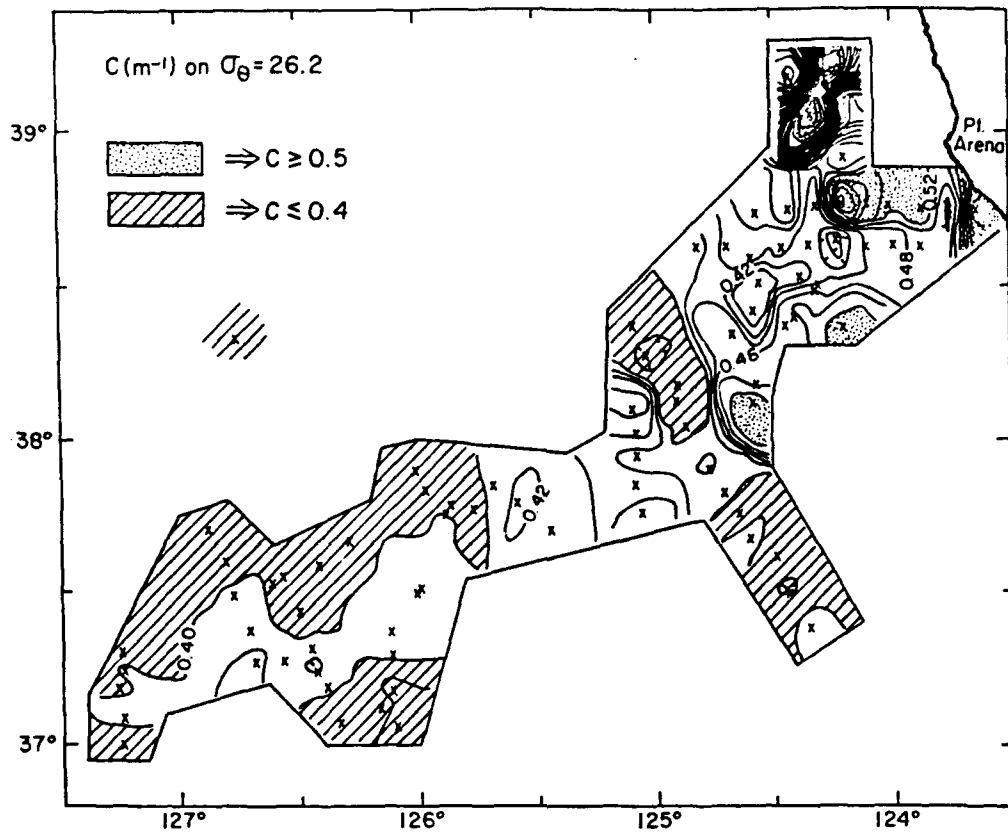


A.

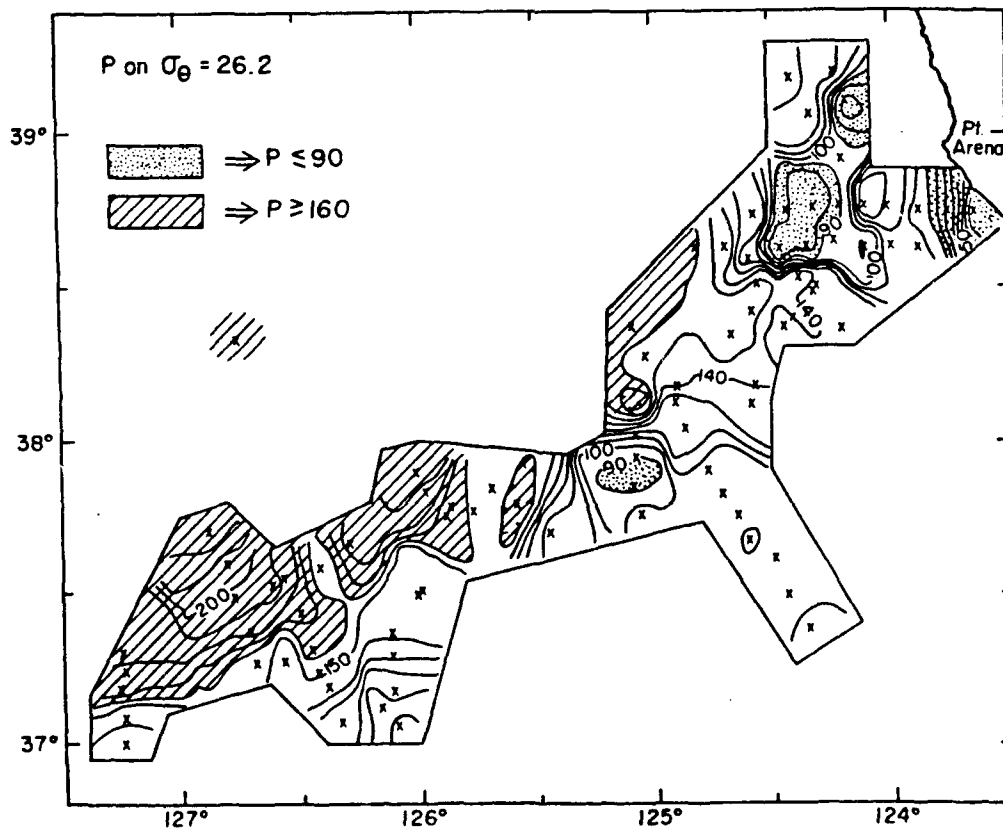


B.

FIG. 7

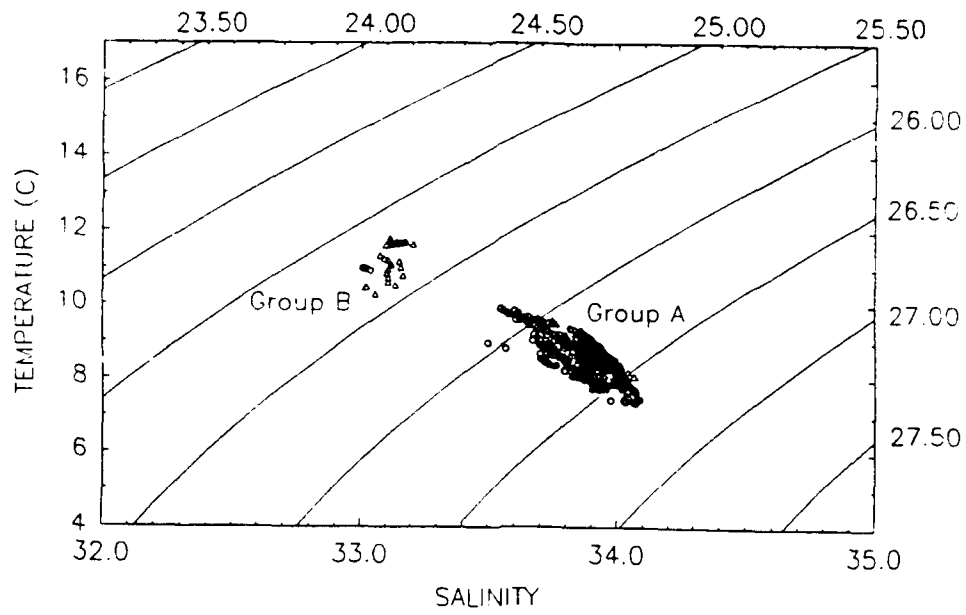


A.

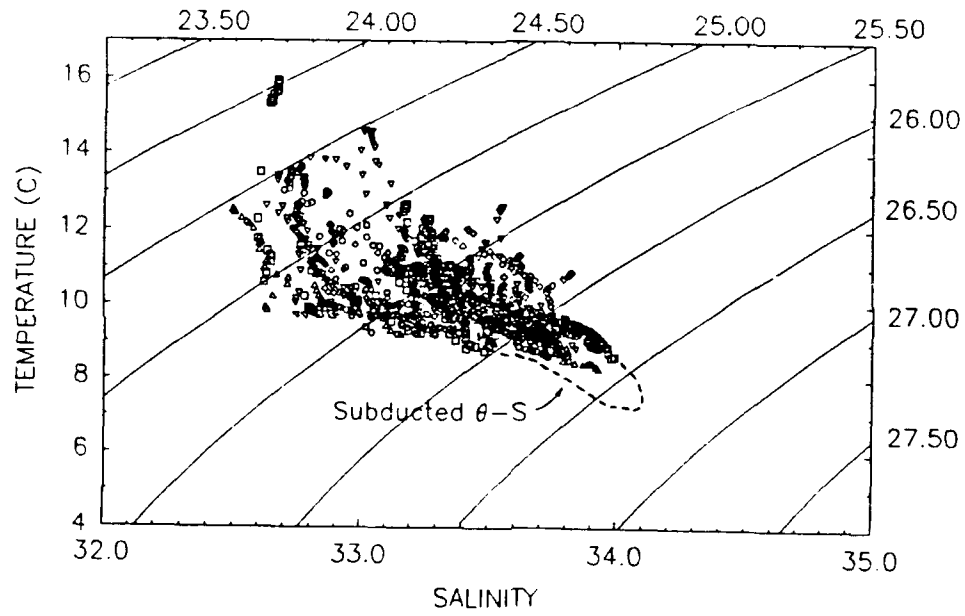


B.

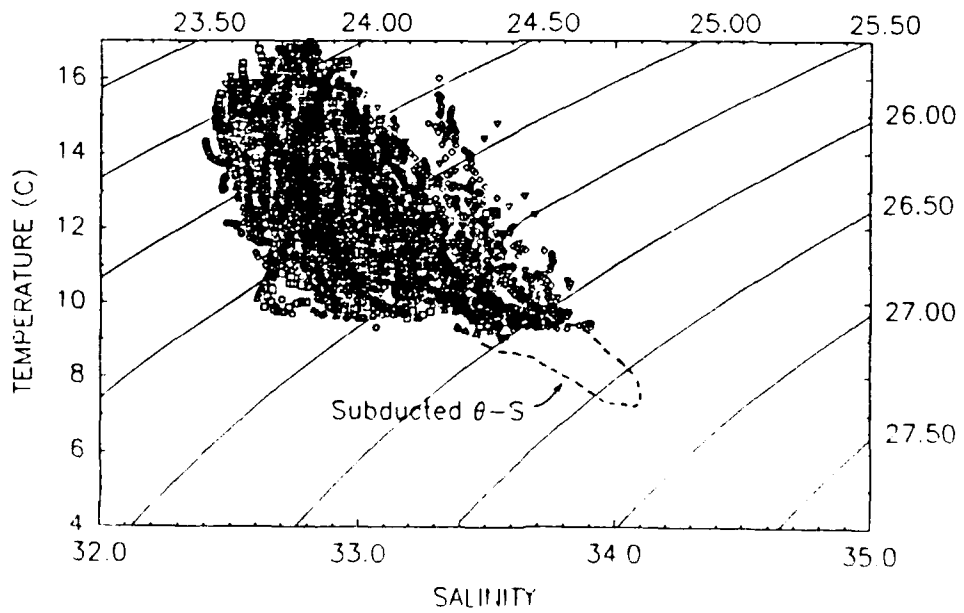
FIG. 8



A.

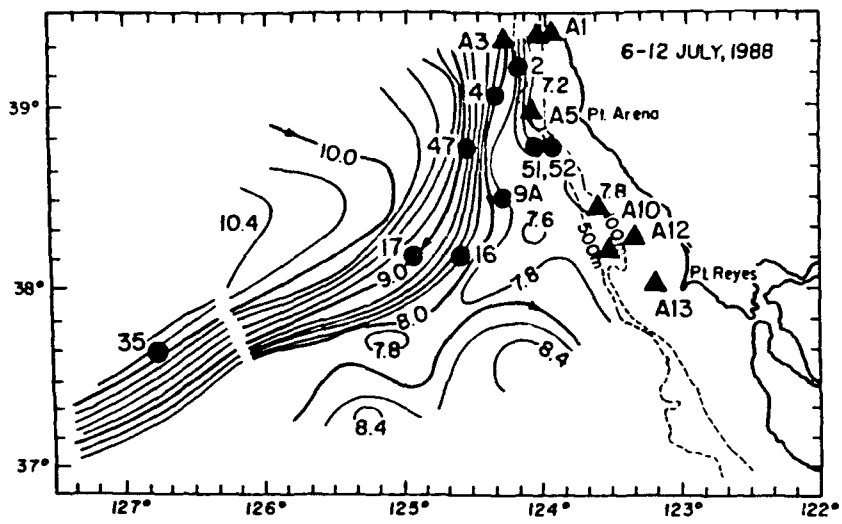


B.

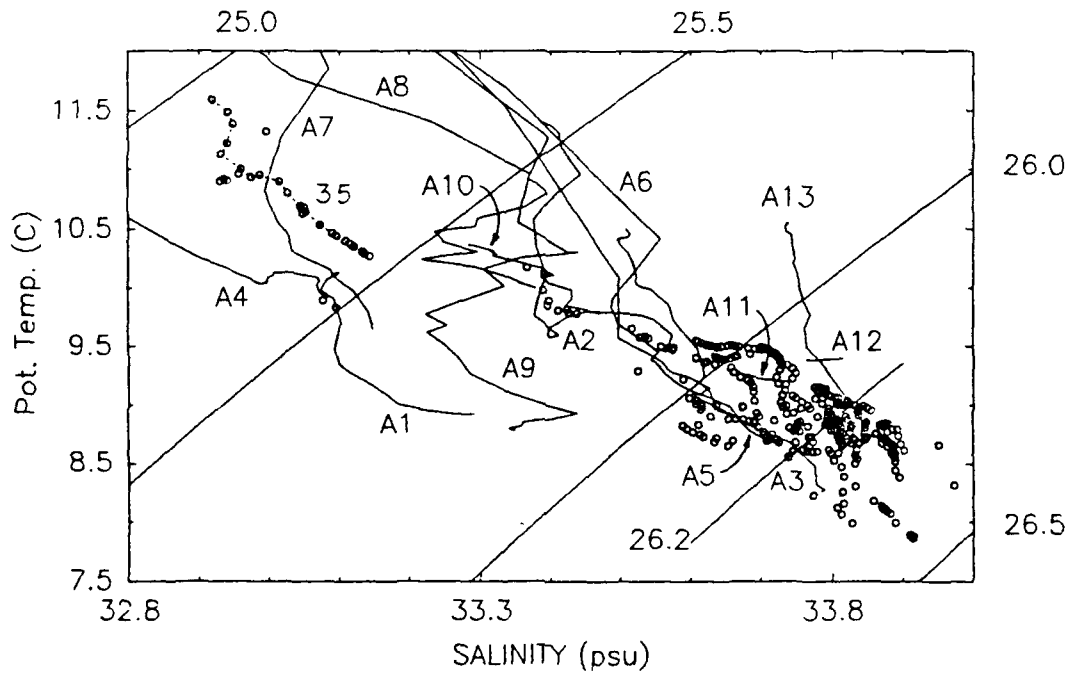


C.

FIG. 9



A.



B.

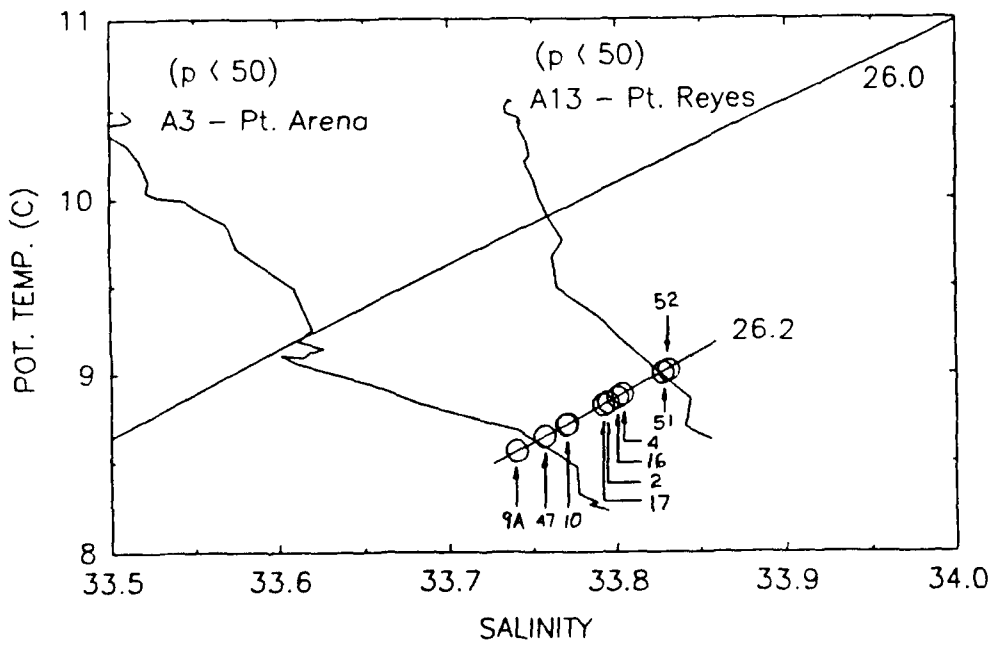


FIG. 10

C.

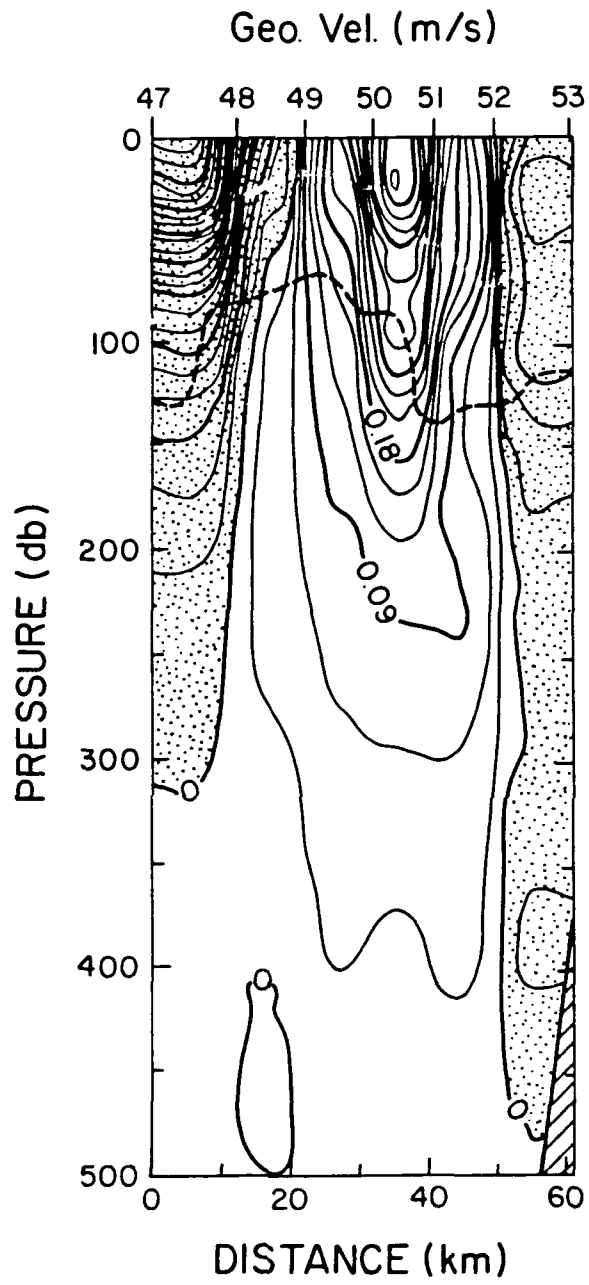


FIG. 11

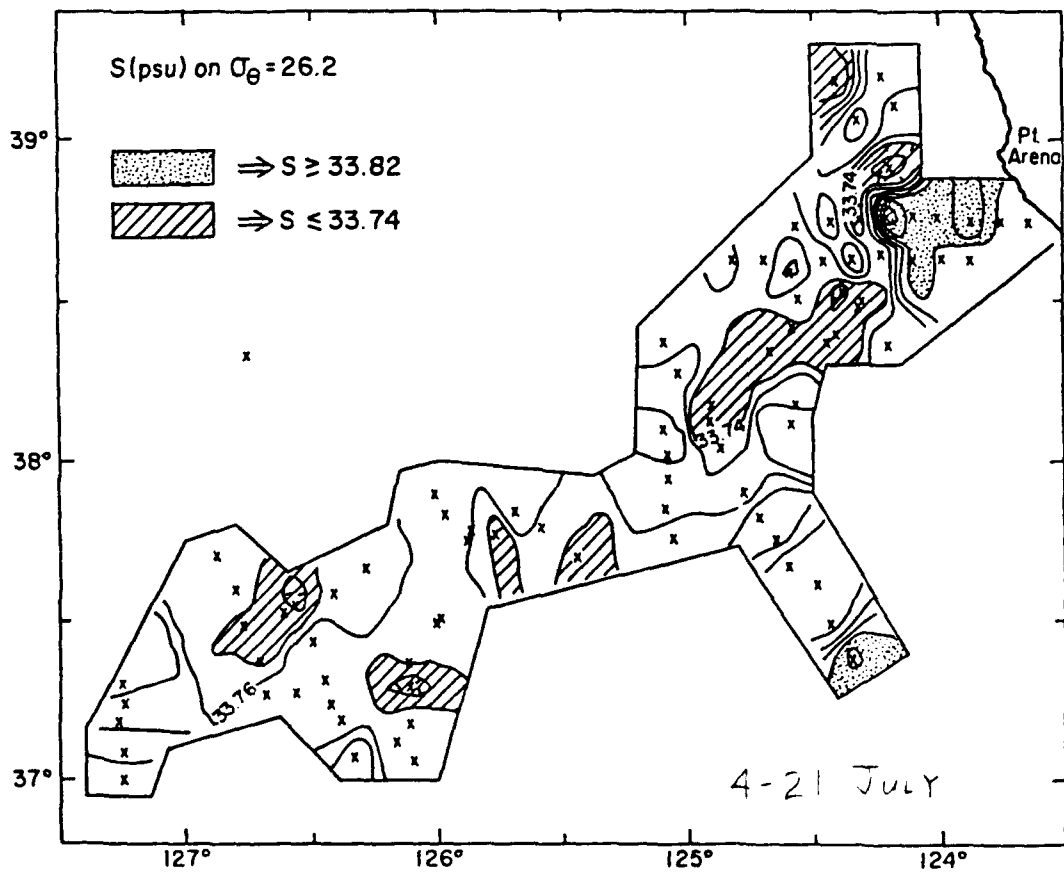
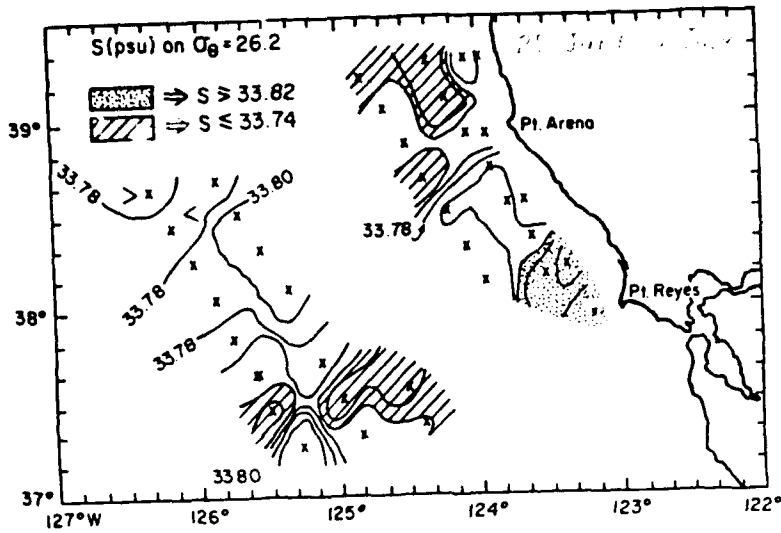
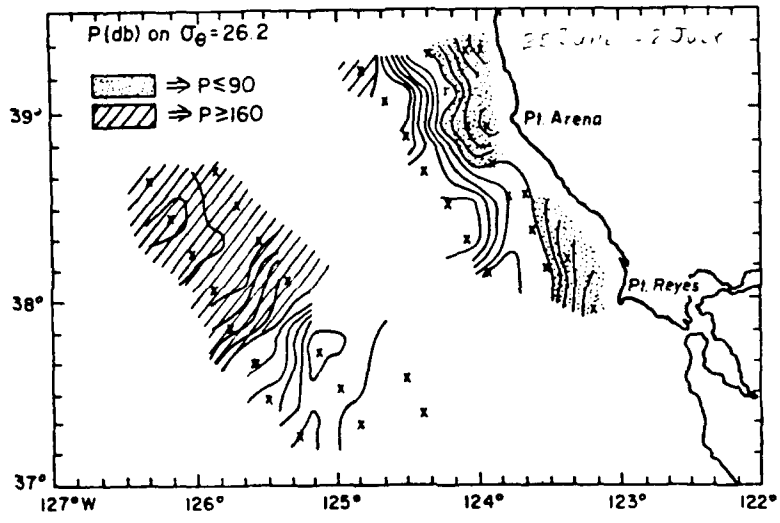


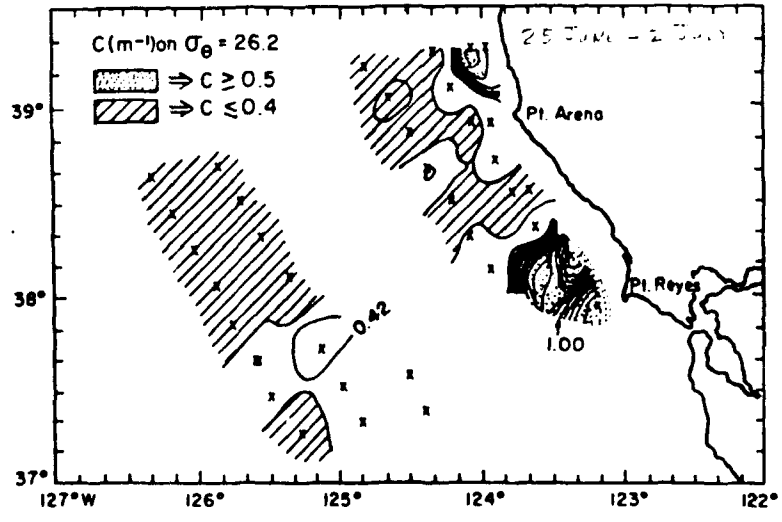
FIG. 12



A.



B.



C.

FIG. 13

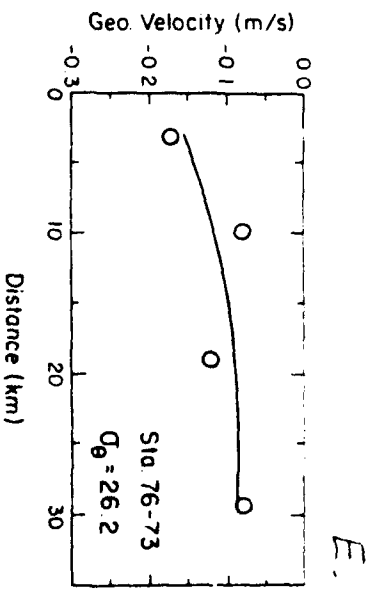
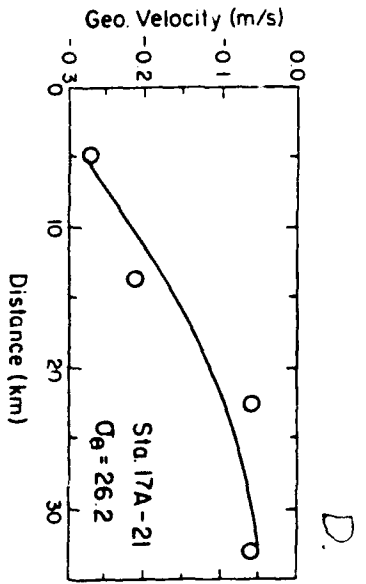
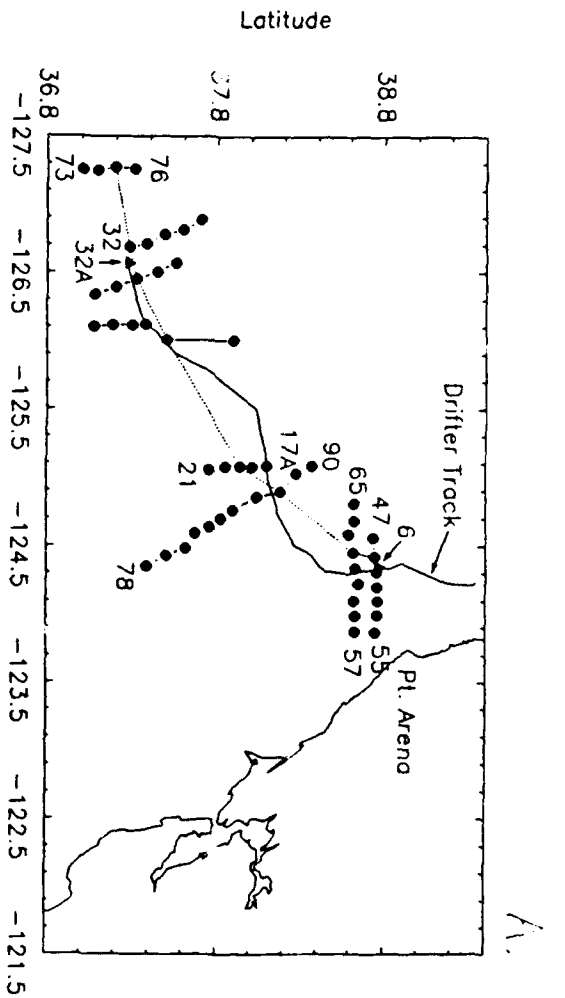
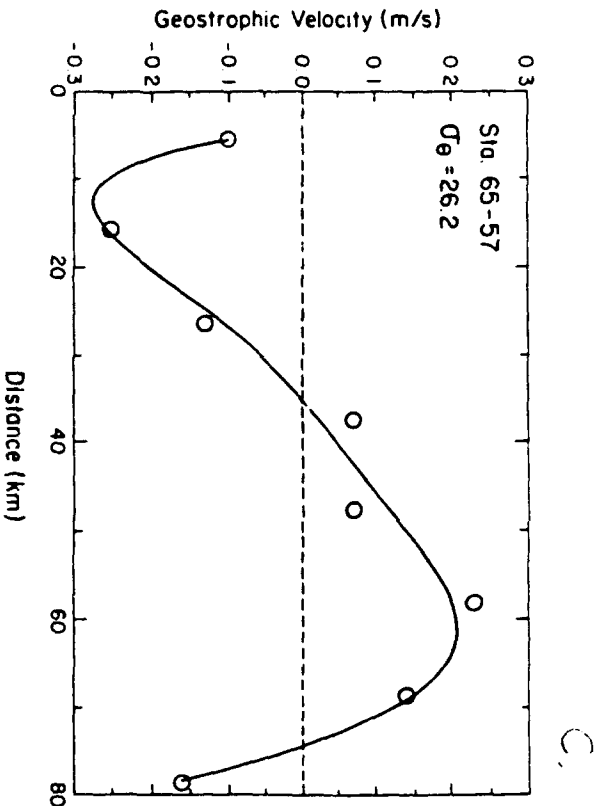
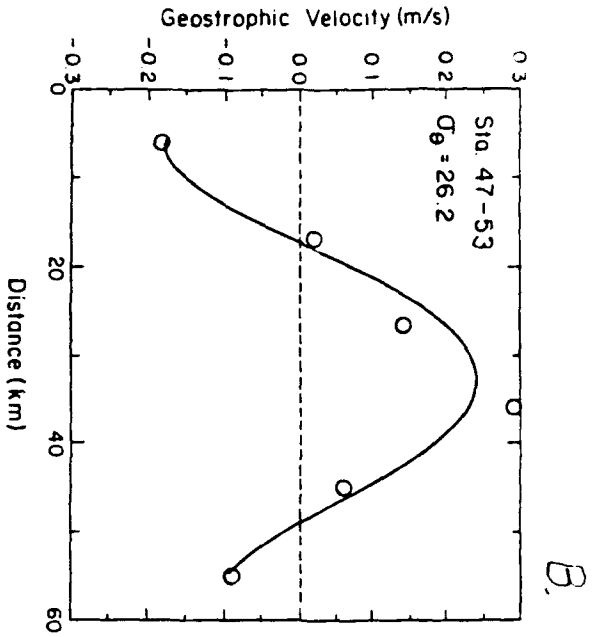


FIG. 14